A general upper bound on the light dark matter scattering rate in materials

Downloaded from: https://research.chalmers.se, 2025-10-14 18:55 UTC

Citation for the original published paper (version of record):
Catena, R., Iglicki, M. (2025). A general upper bound on the light dark matter scattering rate in materials. Journal of Cosmology and Astroparticle Physics, 2025(8). http://dx.doi.org/10.1088/1475-7516/2025/08/088

N.B. When citing this work, cite the original published paper.

research.chalmers.se offers the possibility of retrieving research publications produced at Chalmers University of Technology. It covers all kind of research output: articles, dissertations, conference papers, reports etc. since 2004. research.chalmers.se is administrated and maintained by Chalmers Library

(article starts on next page)

Journal of Cosmology
and Astroparticle
Physics

PAPER • OPEN ACCESS

A general upper bound on the light dark matter scattering rate in materials

To cite this article: Riccardo Catena and Michał Iglicki JCAP08(2025)088

View the article online for updates and enhancements.

You may also like

- Effective field theory approach to leptophilic self-conjugate dark matter
Hrishabh Bharadwaj and Ashok Goyal
- Secluded scalar dark matter and the muon anomalous magnetic moment
Karim Ghorbani
- Spin-dependent sub-GeV inelastic dark matter-electron scattering and Migdal effect. Part I. Velocity independent operator
Jiwei Li, Liangliang Su, Lei Wu et al.

This content was downloaded from IP address 129.16.140.64 on 09/09/2025 at 06:40

Journal of Cosmology and Astroparticle Physics
An IOP and SISSA journal

Received: *February 6, 2025*
Revised: *June 27, 2025*
Accepted: *July 21, 2025*
Published: *August 28, 2025*

A general upper bound on the light dark matter scattering rate in materials

Riccardo Catena and Michał Iglicki

Department of Physics, Chalmers University of Technology, SE-412 96 Göteborg, Sweden

E-mail: catena@chalmers.se, michal.iglicki@chalmers.se

Abstract: Combining an effective theory description of spin-1/2 dark matter (DM)-electron interactions in materials with linear response theory provides a powerful framework to model the scattering of DM, including in-medium effects, in detectors used for direct searches. Within this framework, we show that the rate of DM-induced electronic transitions in detector materials admits a theoretical upper bound under general assumptions on the underlying DM-electron coupling. In particular, our theoretical upper bound applies to models where DM couples to the electron density as well as the spin, paramagnetic and Rashba currents in materials, and arises from the Kramers-Kronig relations that constrain the analytic properties of the scattering rate. We evaluate our maximum rate formula numerically for Ar, Xe, Ge, and Si targets and find that Ge and Si detectors are closer to saturate this theoretical upper bound, but still far from saturation when DM couples to densities or currents which are different from the electron density. This motivates the exploration of a different class of materials to effectively probe such coupling forms.

Keywords: dark matter theory, dark matter detectors

ArXiv ePrint: 2501.18261

© 2025 The Author(s). Published by IOP Publishing Ltd on behalf of Sissa Medialab. Original content from this work may be used under the terms of the Creative Commons Attribution 4.0 licence. Any further distribution of this work must maintain attribution to the author(s) and the title of the work, journal citation and DOI.

https://doi.org/10.1088/1475-7516/2025/08/088

JCAP08(2025)088

Contents

1 Introduction

The quest for dark matter (DM) is gradually broadening its focus, with a remarkable, global experimental effort directed towards probing models where the DM particle is approximately in the MeV to GeV mass range [1–3]. The experimental search for DM particles lighter than a GeV is motivated by the lack of discovery of WIMPs at direct detection experiments, and by the possibility of producing a DM candidate in this mass window with the correct cosmological abundance via the freeze-out mechanism (if the Lee-Weinberg bound [4] is circumvented by introducing the exchange of a new particle mediator in the relevant number-changing processes).

The search for DM-induced electronic transitions in germanium [5] and silicon [6–8], as well as liquid argon [9] and xenon [10], has so far played a major role in the exploration of the MeV to GeV mass window in direct detection experiments. The formalism for describing the scattering of Milky Way, sub-GeV DM particles on the electrons bound to a detector

JCAP08(2025)088

material has been put forward in [11–13], and subsequently extended to account for in-medium screening in models where DM couples to the electron density in the target [14, 15]. More recently, linear response theory has been used to further extend the formalism for DM-electron scattering in materials to effective theories where DM couples to all the electron densities and currents that arise at leading order in the non-relativistic expansion of the DM-electron scattering amplitude [16]. Effective theories for DM-electron interactions have been formulated in [17, 18], as well as in [19, 20].

Focusing on models where fermionic DM couples to the electron density, it has been pointed out that there exists a theoretical upper bound on the rate of DM-induced electronic transitions in a detector [21]. This bound arises from the so-called Kramers-Kronig relations, which follow from the analytic properties of the dielectric function, upon which the DM-induced electronic transition rate depends. This is an interesting observation, because it provides a systematic framework to identify optimal detector materials to probe the DM coupling to the electron density.

In this work, we show that a theoretical upper bound on the rate of spin-1/2 DM-induced electronic transitions exists not only in models where DM couples to the electron density, but also in models where it couples to the paramagnetic current, the spin current, the scalar product of spin and paramagnetic current, and the Rashba spin-orbit current. This extends the results of [21] to the leading currents and densities arising from the non-relativistic expansion of the DM-electron scattering amplitude, or, equivalently, from the non-relativistic expansion of the Dirac Hamiltonian [16]. Analogously to [21], the existence of the upper bound we find here follows from an application of the Kramers-Kronig relations. However, we do not apply the Kramers-Kronig relations to the dielectric function only, but also to the generalized susceptibilities that describe the linear response of materials to the leading, non-relativistic DM-electron couplings. For each given DM coupling, the ratio between the actual DM-induced electronic transition rate and our theoretical upper bound only depends on the assumed detector material and DM mass. For all currents and densities listed above, we evaluate this ratio focusing on Si, Ge, Ar, and Xe as detector materials. In general, we find that Si and Ge are closer to saturate our theoretical upper bound, but still far from saturation in all models where DM couples to densities or currents which are different from the electron number density. This points towards the need for a different class of materials to effectively probe such coupling forms.

Our work is organized as follows. In section 2 we review the use of the Kramers-Kronig relations in the context of DM direct detection, and show why they imply a theoretical upper bound on the rate of DM-induced electronic transitions in models where DM couples to the electron density in the detector. In section 3, we review the application of linear response theory to DM direct detection, and show that, for general DM-material couplings, the rate of DM-induced electronic transitions can be expressed in terms of generalized susceptibilities which, under general conditions, also obey the Kramers-Kronig relations. In section 4.1, we use our generalized susceptibility formalism to obtain a theoretical upper bound on the rate of DM-induced electronic transitions in models where DM couples to the leading, non-relativistic electron densities and currents. In section 4.2, we provide expressions for the interaction rate calculated in some specific effective models of DM-electron interactions. We evaluate our theoretical upper bound in section 4.3, and conclude in section 5. Additional results

JCAP08(2025)088

and useful identities, as well as a short discussion of some assumptions, are collected in the appendices A to D.

2 Electronic transitions induced by a DM-electron density coupling

As already mentioned in the introduction, throughout the whole paper we assume the electrons to be non-relativistic, so that their kinetic energies are much smaller than m_e. Nevertheless, some electrons in the material, namely, those at the innermost atomic shells, may be predominantly relativistic, as their expected kinetic energies are comparable to m_e. Those electrons, however, are tightly bounded to the nucleus and, therefore, difficult to excite. Therefore, they do not significantly contribute to the total excitation rate. The valence electrons, whose excitations would be the main source of the DM-induced signal, are not subject to any significant relativistic corrections [22], so the non-relativistic treatment is justified.

2.1 Fermi's golden rule

The rate of transitions from an electronic state $|i\rangle$ to an electronic state $|f\rangle$, induced by an incoming DM particle of momentum $\boldsymbol{p}$ and a spin configuration s scattering to a final state momentum between $\boldsymbol{p}'$ and $\boldsymbol{p}' + \mathrm{d}\boldsymbol{p}'$ and with a spin configuration s', is given by Fermi's golden rule,

$$\mathrm{d}\Gamma^{ss'}_{i\to f}(\boldsymbol{p}) = (2\pi)\delta(E_f + E_{\boldsymbol{p}'} - E_i - E_{\boldsymbol{p}}) \left|\langle f; \boldsymbol{p}', s'| \, \widehat{V} \, |\boldsymbol{p}, s; i\rangle\right|^2 \frac{V \mathrm{d}\boldsymbol{p}'}{(2\pi)^3} \,, \tag{2.1}$$

where $\widehat{V}$ is the DM-electron interaction potential, E_i (E_f) the energy of the initial (final) electronic state, and $E_{\boldsymbol{p}}$ ($E_{\boldsymbol{p}'}$) the energy of the initial (final) DM particle. Here, single particle states are normalized to one, while $V \equiv \int \mathrm{d}\boldsymbol{x}$ is a normalization volume such that the number of DM particle states with momenta between $\boldsymbol{p}'$ and $\boldsymbol{p}' + \mathrm{d}\boldsymbol{p}'$ in a volume V is $V\mathrm{d}\boldsymbol{p}'/(2\pi)^3$.

In position space, the matrix element of the interaction potential $\widehat{V}$ can be written as follows,

$$\langle f; \boldsymbol{p}', s'|\widehat{V}|\boldsymbol{p}, s; i\rangle = \frac{1}{V} \int \mathrm{d}\boldsymbol{r}_e \int \mathrm{d}\boldsymbol{r}_\chi \, \psi^*_f(\boldsymbol{r}_e) \, e^{-i\boldsymbol{p}'\cdot\boldsymbol{r}_\chi} \, \xi^{s'\dagger}_\chi \widehat{V}_x(\boldsymbol{r}_e, \boldsymbol{r}_\chi, \dots) \xi^s_\chi \, e^{i\boldsymbol{p}\cdot\boldsymbol{r}_\chi} \, \psi_i(\boldsymbol{r}_e) \,, \tag{2.2}$$

where we have assumed spin-1/2 DM and ξ^s_χ (ξ^s_χ) is a two-component spinor describing the spin configuration of the initial (final) DM particle (i.e., up or down for spin-1/2 DM), ψ_i (ψ_f) is the initial (final) electronic wave function, while $\widehat{V}_x$ denotes the position space interaction potential. The dots in eq. (2.2) denote gradient and spin operators which $\widehat{V}_x$ can in general depend on. In eq. (2.2), we integrate over the electron and DM particle position vectors, $\boldsymbol{r}_e$ and $\boldsymbol{r}_\chi$.

By assuming $\widehat{V}_x(\boldsymbol{r}_e, \boldsymbol{r}_\chi, \dots) = \mathbb{1}_e \mathbb{1}_\chi \widehat{V}_x(\boldsymbol{r}_e - \boldsymbol{r}_\chi)$ (which applies to the case of velocity- and spin-independent interactions), where $\mathbb{1}_e$ ($\mathbb{1}_\chi$) is the 2×2 identity in the electron (DM particle) spin space, the matrix element in eq. (2.2) can now be rewritten as follows,

$$\begin{aligned} \langle f; \boldsymbol{p}', s'|\widehat{V}|\boldsymbol{p}, s; i\rangle &= \int \mathrm{d}\boldsymbol{r}_e \, \psi^*_f(\boldsymbol{r}_e) V^{ss'}_{\mathrm{eff}}(\boldsymbol{r}_e, \boldsymbol{q}) \, \psi_i(\boldsymbol{r}_e) \\ &= \langle f| \, V^{ss'}_{\mathrm{eff}} \, |i\rangle \,, \end{aligned} \tag{2.3}$$

JCAP08(2025)088

where

$$V_{\rm eff}^{ss'}(\boldsymbol{r}_e, \boldsymbol{q}) \equiv \frac{1}{V} e^{i\boldsymbol{q}\cdot\boldsymbol{r}_e}\, \mathbb{1}_e\, \delta^{ss'} \widetilde{V}_x(\boldsymbol{q})\,, \tag{2.4}$$

is the effective transition potential,

$$\widetilde{V}_x(\boldsymbol{q}) \equiv \int \mathrm{d}\,(\boldsymbol{r}_e - \boldsymbol{r}_\chi)\; e^{-i\boldsymbol{q}\cdot(\boldsymbol{r}_e - \boldsymbol{r}_\chi)}\, \widehat{V}_x(\boldsymbol{r}_e - \boldsymbol{r}_\chi)\,, \tag{2.5}$$

and $\boldsymbol{q} = \boldsymbol{p} - \boldsymbol{p}'$ is the momentum transfer. Recalling that the number density of an electron at $\boldsymbol{r}_e$ and its Fourier transform at $\boldsymbol{q}$ are given by

$$n_0(\boldsymbol{r}) = \delta^{(3)}(\boldsymbol{r} - \boldsymbol{r}_e)\,, \qquad\qquad \widetilde{n}_0(\boldsymbol{q}) = e^{-i\boldsymbol{q}\cdot\boldsymbol{r}_e}\,, \tag{2.6}$$

we find that

$$V_{\rm eff}^{ss'}(\boldsymbol{r}_e, \boldsymbol{q}) \equiv \frac{1}{V}\, \widetilde{n}_0(-\boldsymbol{q})\, \mathbb{1}_e\, \delta^{ss'} \widetilde{V}_x(\boldsymbol{q})\,. \tag{2.7}$$

Independently of the specific form of $\widetilde{V}_x(\boldsymbol{q})$, whenever $\widehat{V}_x(\boldsymbol{r}_e, \boldsymbol{r}_\chi, \dots) = \mathbb{1}_e \mathbb{1}_\chi \widehat{V}_x(\boldsymbol{r}_e - \boldsymbol{r}_\chi)$ the transition potential $V_{\rm eff}^{ss'}(\boldsymbol{r}_e, \boldsymbol{q})$ depends on the properties of the electrons bound to the target material through the electron density solely. One can summarize this property of the underlying DM-electron interaction by saying that the DM couples to the electron density in the material.

As an example, let us consider the following amplitude for DM scattering by free electrons,

$$\mathscr{M} = c_1\, \delta^{ss'} \delta^{rr'}\,, \tag{2.8}$$

where c_1 is a dimensionless constant, while r (r') labels the initial (final) state electron spin. In the Born approximation, the relation between $\mathscr{M}$ and the associated scattering potential is

$$\langle \boldsymbol{k}', r'; \boldsymbol{p}', s' | \widehat{V} | \boldsymbol{p}, s; \boldsymbol{k}, r \rangle = -(2\pi)^3 \delta^{(3)}(\boldsymbol{p}' + \boldsymbol{k}' - \boldsymbol{k} - \boldsymbol{p})\, \frac{\mathscr{M}}{4 m_e m_\chi V^2}\,, \tag{2.9}$$

where $\boldsymbol{k}$ ($\boldsymbol{k}'$) is the initial (final) free electron momentum. By inserting eq. (2.2) with free electron wave functions $\psi_i(\boldsymbol{r}_e) = \xi_e^r e^{i\boldsymbol{k}\cdot\boldsymbol{r}_e}/\sqrt{V}$ and $\psi_f(\boldsymbol{r}_e) = \xi_e^{r'} e^{i\boldsymbol{k}'\cdot\boldsymbol{r}_e}/\sqrt{V}$ into eq. (2.9), we obtain

$$\widehat{V}_x(\boldsymbol{r}_e - \boldsymbol{r}_\chi) = -\frac{c_1}{4 m_e m_\chi}\, \delta^{(3)}(\boldsymbol{r}_e - \boldsymbol{r}_\chi)\,, \tag{2.10}$$

and, using eq. (2.7),

$$V_{\rm eff}^{ss'}(\boldsymbol{r}_e, \boldsymbol{q}) = -\frac{c_1}{4 m_e m_\chi V}\, \delta^{ss'}\, \mathbb{1}_e\, \widetilde{n}_0(-\boldsymbol{q})\,. \tag{2.11}$$

2.2 Dielectric function formalism

By inserting eq. (2.3), with $V_{\rm eff}^{ss'}(\boldsymbol{r}_e, \boldsymbol{q})$ given in eq. (2.7), into eq. (2.1), we find the rate formula

$$\mathrm{d}\Gamma_{i\to f}^{ss'}(\boldsymbol{p}) = \frac{(2\pi)}{V}\, \delta(E_f + E_{\boldsymbol{p}'} - E_i - E_{\boldsymbol{p}})\, \delta^{ss'}\, |\widetilde{V}_x(\boldsymbol{q})|^2\; |\langle f|\, \widetilde{n}_0(-\boldsymbol{q})\, |i\rangle|^2\; \frac{\mathrm{d}\boldsymbol{p}'}{(2\pi)^3}\,. \tag{2.12}$$

JCAP08(2025)088

Summing (averaging) over the final (initial) electronic configurations and DM particle spins, and averaging over the initial DM particle velocities $\boldsymbol{v} = \boldsymbol{p}/m_\chi$ (defined in the laboratory frame), we can now calculate the total electronic transition rate induced by a galactic DM particle whose initial velocity in the laboratory frame is distributed according to the probability density $f(\boldsymbol{v})$, and whose final momentum lies between $\boldsymbol{p}'$ and $\boldsymbol{p}' + \mathrm{d}\boldsymbol{p}'$. In addition, by integrating over the final DM momenta $\boldsymbol{p}'$ or, equivalently, over the momentum transfer $\boldsymbol{q}$, we find

$$\Gamma = \frac{1}{2}\sum_{ss'}\sum_{if}\frac{e^{-\beta E_i}}{Z}\int \mathrm{d}\boldsymbol{v}\, f(\boldsymbol{v})\int \mathrm{d}\boldsymbol{q}\,\frac{\mathrm{d}\Gamma^{ss'}_{i\to f}(\boldsymbol{p})}{\mathrm{d}\boldsymbol{q}}\,, \tag{2.13}$$

where Z is the partition function, $\beta = 1/T$, and T denotes the temperature (in DM direct detection applications, $T \to 0$; see appendix D.2 for a short discussion). Introducing $K_{n_0 n_0}(\boldsymbol{q},\omega)$, the density-density correlation function,

$$K_{n_0 n_0}(\boldsymbol{q},\omega) = \frac{2\pi}{V}\sum_{if}\frac{e^{-\beta E_i}}{Z}\,\langle f|\widetilde{n}_0(-\boldsymbol{q})|i\rangle\,\langle i|\widetilde{n}_0(\boldsymbol{q})|f\rangle\,\delta(E_f - E_i - \omega)\,, \tag{2.14}$$

we can rewrite Γ as

$$\Gamma = \int\frac{\mathrm{d}\boldsymbol{q}}{(2\pi)^3}\,|\widetilde{V}_x(\boldsymbol{q})|^2\int \mathrm{d}\boldsymbol{v}\, f(\boldsymbol{v})\, K_{n_0 n_0}(\boldsymbol{q},\omega_{\boldsymbol{v},\boldsymbol{q}})\,, \tag{2.15}$$

where

$$\omega_{\boldsymbol{v},\boldsymbol{q}} = E_{\boldsymbol{p}} - E_{\boldsymbol{p}-\boldsymbol{q}} = \boldsymbol{q}\cdot\boldsymbol{v} - \frac{q^2}{2m_\chi}\,. \tag{2.16}$$

Finally, by using [16][1]

$$K_{n_0 n_0}(\boldsymbol{q},\omega) = \frac{2}{1-e^{-\beta\omega}}\,\mathrm{Im}\left[-\varepsilon_r(\boldsymbol{q},\omega)^{-1}\right]\,U(q)^{-1}\,, \tag{2.17}$$

where $U(q) = 4\pi\alpha/q^2$ is the Fourier transform of the Coulomb potential and α the fine structure constant, we obtain

$$\Gamma = \int\frac{\mathrm{d}\boldsymbol{q}}{(2\pi)^3}\,|\widetilde{V}_x(\boldsymbol{q})|^2\int \mathrm{d}\boldsymbol{v}\, f(\boldsymbol{v})\,\frac{2}{1-e^{-\beta\omega_{\boldsymbol{v},\boldsymbol{q}}}}\,\mathrm{Im}\left[-\varepsilon_r(\boldsymbol{q},\omega_{\boldsymbol{v},\boldsymbol{q}})^{-1}\right]\,U(q)^{-1}\,, \tag{2.18}$$

which gives a formula for the DM-induced electronic transition rate in terms of the dielectric function $\varepsilon_r(\boldsymbol{q},\omega)$ (defined as in [23]). Eq. (2.18) applies to models where DM couples to the electron density in materials.

2.3 Kramers-Kronig relations

By combining the dielectric function formalism reviewed above with the Kramers-Kronig relations, one can derive a theoretical upper bound on Γ in models where DM couples to the electron density in materials [21]. To show this, let us first introduce the Kramers-Kronig relations.

[1]The local field effects, discussed in [16], are neglected here.

JCAP08(2025)088

Let function $g : \mathbb{C} \to \mathbb{C}$ be analytic in the upper half plane,[2] and $g(z) \to 0$ for $|z| \to \infty$. Then, g must satisfy the following Kramers-Kronig relations [23]:

$$\mathrm{Re}\, g(z_0) = \frac{1}{\pi}\mathcal{P}\int_{-\infty}^{+\infty} \frac{\mathrm{d}z}{z - z_0}\, \mathrm{Im}\, g(z)\,, \tag{2.19a}$$

$$\mathrm{Im}\, g(z_0) = -\frac{1}{\pi}\mathcal{P}\int_{-\infty}^{+\infty} \frac{\mathrm{d}z}{z - z_0}\, \mathrm{Re}\, g(z)\,, \tag{2.19b}$$

where $\mathcal{P}$ denotes the principal value. In particular, for $z_0 = 0$, we obtain

$$\mathrm{Re}\, g(0) = \frac{1}{\pi}\mathcal{P}\int_{-\infty}^{+\infty} \frac{\mathrm{d}z}{z}\, \mathrm{Im}\, g(z)\,, \tag{2.20a}$$

$$\mathrm{Im}\, g(0) = -\frac{1}{\pi}\mathcal{P}\int_{-\infty}^{+\infty} \frac{\mathrm{d}z}{z}\, \mathrm{Re}\, g(z)\,. \tag{2.20b}$$

If, in addition, g satisfies a third property — namely, that its Fourier transform is real[3] — its real part $\mathrm{Re}\, g(z)$ is even and its imaginary part $\mathrm{Im}\, g(z)$ is odd as a function of $z \in \mathbb{R}$. Then, eq. (2.20a) becomes

$$\int_0^{+\infty} \frac{\mathrm{d}z}{z}\, \mathrm{Im}\, g(z) = \frac{\pi}{2} g(0)\,. \tag{2.21}$$

Since $1 - \varepsilon_r(\boldsymbol{q}, \omega)^{-1}$ as a function of ω obeys the above three conditions for each $\boldsymbol{q}$, one can write

$$\int_0^{+\infty} \frac{\mathrm{d}\omega}{\omega}\, \mathrm{Im}\left[1 - \varepsilon_r(\boldsymbol{q}, \omega)^{-1}\right] = \frac{\pi}{2}\left[1 - \varepsilon_r(\boldsymbol{q}, 0)^{-1}\right]\,. \tag{2.22}$$

This identity implies a theoretical upper bound on the rate of DM-induced electronic transitions Γ [21]. Indeed, in eq. (2.18), the change of integration variables introduced in appendix B leads to

$$\Gamma = \int_0^{\infty} \mathrm{d}q\, \frac{q^2\, U(q)^{-1}}{2\pi^2}\, |\widetilde{V}_x(q)|^2 \int_0^{\infty} \mathrm{d}\omega\, \rho^{(0)}(\omega, q)\, \frac{2}{1 - e^{-\beta\omega}}\, \mathrm{Im}\left[-\varepsilon_r(q, \omega)^{-1}\right]\,, \tag{2.23}$$

where

$$\rho^{(0)}(\omega, q) = \frac{\pi}{q}\int_{v_q}^{\infty} \mathrm{d}v\, v \int_{-1}^{1} \mathrm{d}\cos\alpha\, f(\boldsymbol{v})\,. \tag{2.24}$$

Here, we assume

$$\begin{aligned} f(\boldsymbol{v}) &= f(v, \cos\alpha) \\ &= \mathcal{N}\, \exp\left[-\frac{(\boldsymbol{v} + \boldsymbol{v}_\oplus)^2}{v_0^2}\right]\, \theta(v_{\mathrm{esc}} - |\boldsymbol{v} + \boldsymbol{v}_\oplus|)\,, \end{aligned} \tag{2.25}$$

where $\boldsymbol{v} \cdot \boldsymbol{v}_\oplus = v v_\oplus \cos\alpha$, $\boldsymbol{v}_\oplus$ is Earth's velocity relative to the galactic centre, v_{esc} is the galactic escape velocity, v_0 is the most probable DM speed (in the galactic reference frame,

[2] This is satisfied if the Fourier transform of g is proportional to the step function. Physically, it means that if z denotes frequency, the Fourier transform of g is causal as a function of time.

[3] For example, if z is frequency, then this third condition requires the function g to be real in the time domain.

JCAP08(2025)088

in which the mean DM velocity is zero), while $\mathcal{N}$ is a normalization constant. The assumed values of $v_\oplus \equiv |\boldsymbol{v}_\oplus|$, $v_{\rm esc}$, v_0, and $\mathcal{N}$ are listed in appendix A. We also introduce the minimum DM speed required to deposit an energy ω,

$$\begin{aligned} v_q &\equiv \boldsymbol{v} \cdot \frac{\boldsymbol{q}}{q} \\ &= \frac{\omega}{q} + \frac{q}{2\,m_\chi}\,, \end{aligned} \tag{2.26}$$

and assume an isotropic target (equivalently: average over detector's orientations, see appendix D.1 for a short discussion), so that we can ignore the dependence of ε_r on the direction of $\boldsymbol{q}$,[4]

$$\varepsilon_r(\boldsymbol{q},\omega) \simeq \varepsilon_r(q,\omega)\,. \tag{2.27}$$

Eqs. (2.22) and (2.23) can now be combined to obtain a theoretical upper bound, $\Gamma_{\rm opt}$, on Γ [21]:

$$\Gamma \leq \Gamma_{\rm opt} = \int_0^\infty {\rm d}q\, \frac{q^2\, U(q)^{-1}}{2\pi}\, |\widetilde{V}_x(q)|^2 \max_\omega \left[\omega \rho^{(0)}(\omega,q)\right]\,, \tag{2.28}$$

where we took into account that for $T \to 0$, $1 - e^{-\beta\omega} \to 1$, and, following [21], assumed $1 - \varepsilon_r(q,0)^{-1} \leq 1$ and ${\rm Im}[-\varepsilon_r(q,\omega)^{-1}] \geq 0$.

3 Electronic transitions induced by general DM-electron couplings

3.1 Fermi's golden rule

In general, DM can couple to electron densities and currents in materials that are different from the electron number density n_0. Specifically, the most general form for the transition potential $V_{\rm eff}^{ss'}$ at leading order in the electron velocity and in the momentum transfer is given by [16]

$$\begin{aligned} V_{\rm eff}^{ss'}(\boldsymbol{r}_e,\boldsymbol{q}) = -\frac{1}{4 m_e m_\chi V} \Bigg\{ & F_{n_0}^{ss'}\, e^{i\boldsymbol{q}\cdot\boldsymbol{r}_e}\, \mathbb{1}_e \\ & + F_{n_A}^{ss'}\, \frac{i}{2m_e} \left[\overleftarrow{\nabla}_{\boldsymbol{r}_e} \cdot \boldsymbol{\sigma}_e\, e^{i\boldsymbol{q}\cdot\boldsymbol{r}_e} - e^{i\boldsymbol{q}\cdot\boldsymbol{r}_e}\, \boldsymbol{\sigma}_e \cdot \overrightarrow{\nabla}_{\boldsymbol{r}_e}\right] \\ & + \boldsymbol{F}_{\boldsymbol{j}_5}^{ss'} \cdot \boldsymbol{\sigma}_e\, e^{i\boldsymbol{q}\cdot\boldsymbol{r}_e} \\ & + \boldsymbol{F}_{\boldsymbol{j}_M}^{ss'} \cdot \frac{i}{2m_e} \left[\overleftarrow{\nabla}_{\boldsymbol{r}_e} e^{i\boldsymbol{q}\cdot\boldsymbol{r}_e} - e^{i\boldsymbol{q}\cdot\boldsymbol{r}_e} \overrightarrow{\nabla}_{\boldsymbol{r}_e}\right] \mathbb{1}_e \\ & + \boldsymbol{F}_{\boldsymbol{j}_E}^{ss'} \cdot \frac{1}{2m_e} \left[\overleftarrow{\nabla}_{\boldsymbol{r}_e} \times \boldsymbol{\sigma}_e\, e^{i\boldsymbol{q}\cdot\boldsymbol{r}_e} + e^{i\boldsymbol{q}\cdot\boldsymbol{r}_e}\, \boldsymbol{\sigma}_e \times \overrightarrow{\nabla}_{\boldsymbol{r}_e}\right] \Bigg\}\,, \end{aligned} \tag{3.1}$$

where an arrow on the gradient operator indicates whether it acts on the initial ($\overrightarrow{\nabla}_{\boldsymbol{r}_e}$) or final ($\overleftarrow{\nabla}_{\boldsymbol{r}_e}$) electron wave function, while the pre-factors $F_{n_0}^{ss'}$, $F_{n_A}^{ss'}$, $\boldsymbol{F}_{\boldsymbol{j}_5}^{ss'}$, $\boldsymbol{F}_{\boldsymbol{j}_M}^{ss'}$, and $\boldsymbol{F}_{\boldsymbol{j}_E}^{ss'}$ are model dependent. These pre-factors are listed in appendix C for the effective theory of

[4] If DM couples to the electron density solely, invariance under three-dimensional rotations implies $\widetilde{V}_x(\boldsymbol{q}) = \widetilde{V}_x(q)$.

JCAP08(2025)088

DM-electron interactions of [17, 18] and in sections 4.2.1 to 4.2.3 for specific models where DM has as an anapole, electric dipole, or magnetic dipole moment.

The first line in eq. (3.1) corresponds to the already discussed case of models where DM couples to the electron number density in materials. The third and fourth lines describe a coupling between DM and the electron spin or paramagnetic current, respectively. The second line can be identified with the spin-paramagnetic current coupling, and the last line with the Rashba term arising at second order in the $1/c$ expansion of the Dirac Hamiltonian [16].

Inserting eq. (3.1) into eq. (2.3), and then the latter into Fermi's golden rule, eq. (2.1), we obtain the following expression for the rate of DM-induced electronic transitions in materials,

$$\Gamma = \frac{1}{16 m_e^2 m_\chi^2} \sum_{ab} \int \frac{\mathrm{d}\boldsymbol{q}}{(2\pi)^3} \int \mathrm{d}\boldsymbol{v}\, f(\boldsymbol{v})\, \mathcal{F}_{ab}(\boldsymbol{q}, \boldsymbol{v}) K_{b^\dagger a}(\boldsymbol{q}, \omega_{\boldsymbol{v},\boldsymbol{q}})\,, \tag{3.2}$$

where

$$\mathcal{F}_{ab}(\boldsymbol{q}, \boldsymbol{v}) = \frac{1}{2} \sum_{ss'} F_a^{ss'}(\boldsymbol{q}, \boldsymbol{v})\, F_b^{ss'*}(\boldsymbol{q}, \boldsymbol{v})\,, \tag{3.3}$$

and $K_{b^\dagger a}(\boldsymbol{q}, \omega)$ is the correlation function,

$$K_{b^\dagger a}(\boldsymbol{q}, \omega) = \frac{2\pi}{V} \sum_{if} \frac{e^{-\beta E_i}}{Z} \langle f | \widetilde{a}(-\boldsymbol{q}) | i \rangle \langle i | \widetilde{b}^\dagger(\boldsymbol{q}) | f \rangle\, \delta(E_f - E_i - \omega)\,, \tag{3.4}$$

while a and b could be any of the densities, or components of currents, contributing to eq. (3.1), namely

$$(\widetilde{n}_0,\ \widetilde{n}_A,\ \widetilde{j}_{5_1},\ \widetilde{j}_{5_2},\ \widetilde{j}_{5_3},\ \widetilde{j}_{M_1},\ \dots\ \widetilde{j}_{E_1},\ \dots)\,, \tag{3.5}$$

where

$$\widetilde{n}_0(\boldsymbol{q}) \equiv e^{-i\boldsymbol{q}\cdot\boldsymbol{r}_e}\,, \tag{3.6a}$$

$$\widetilde{n}_A(\boldsymbol{q}) \equiv \frac{i}{2m_e} \left[\overleftarrow{\nabla}_{\boldsymbol{r}_e} \cdot \boldsymbol{\sigma}_e\, e^{-i\boldsymbol{q}\cdot\boldsymbol{r}_e} - e^{-i\boldsymbol{q}\cdot\boldsymbol{r}_e}\, \boldsymbol{\sigma}_e \cdot \overrightarrow{\nabla}_{\boldsymbol{r}_e} \right]\,, \tag{3.6b}$$

$$\widetilde{\boldsymbol{j}}_5(\boldsymbol{q}) \equiv \boldsymbol{\sigma}_e\, e^{-i\boldsymbol{q}\cdot\boldsymbol{r}_e}\,, \tag{3.6c}$$

$$\widetilde{\boldsymbol{j}}_M(\boldsymbol{q}) \equiv \frac{i}{2m_e} \left[\overleftarrow{\nabla}_{\boldsymbol{r}_e} e^{-i\boldsymbol{q}\cdot\boldsymbol{r}_e} - e^{-i\boldsymbol{q}\cdot\boldsymbol{r}_e} \overrightarrow{\nabla}_{\boldsymbol{r}_e} \right]\,, \tag{3.6d}$$

$$\widetilde{\boldsymbol{j}}_E(\boldsymbol{q}) \equiv \frac{1}{2m_e} \left[\overleftarrow{\nabla}_{\boldsymbol{r}_e} \times \boldsymbol{\sigma}_e\, e^{-i\boldsymbol{q}\cdot\boldsymbol{r}_e} + e^{-i\boldsymbol{q}\cdot\boldsymbol{r}_e}\, \boldsymbol{\sigma}_e \times \overrightarrow{\nabla}_{\boldsymbol{r}_e} \right]\,. \tag{3.6e}$$

We denote by $\boldsymbol{\sigma}_e = (\sigma_1, \sigma_2, \sigma_3)$ the three-dimensional vector whose components are the Pauli matrices. For increased readability, in the remaining part of this work, we omit the tildes (e.g., we write n_0 instead of $\widetilde{n}_0$). In other words, all the densities and currents are hereafter meant to be expressed in momentum space.

3.2 Generalized susceptibility formalism

As the density-density correlation function $K_{n_0 n_0}$ in eq. (2.17) is related to the dielectric function, so is the correlation function $K_{b^\dagger a}$ related to generalized susceptibilities describing the linear response of materials to a perturbation induced by general DM-electron couplings [16].

JCAP08(2025)088

Indeed, in the interaction picture, $V_{\rm eff}^{ss'}$ can be written as a time dependent perturbation [16]:

$$V_{\rm eff}^{ss'}(t) = -\sum_a \int \mathrm{d}\boldsymbol{r}\, B_a(\boldsymbol{r})\, S_a^{ss'}(\boldsymbol{r},t)\,, \tag{3.7}$$

with

$$B_a(\boldsymbol{r}) = \int \frac{\mathrm{d}\boldsymbol{q}'}{(2\pi)^3}\, e^{i\boldsymbol{q}'\cdot\boldsymbol{r}}\, a(\boldsymbol{q}')\,, \tag{3.8}$$

and

$$S_a^{ss'}(\boldsymbol{r},t) = \frac{1}{4m_e m_\chi V}\, F_a^{ss'}\, e^{i\boldsymbol{q}\cdot\boldsymbol{r}}\, e^{-i\omega_{\boldsymbol{v},\boldsymbol{q}}t}\,. \tag{3.9}$$

Notice that at $t = 0$ eqs. (3.1) and (3.7) coincide. In linear response theory, the fluctuation, $\langle \Delta a(\boldsymbol{r},t)\rangle$, induced on the generic electron density or component a by the potential $V_{\rm eff}^{ss'}(t)$ is given by

$$\langle \Delta a(\boldsymbol{r},t)\rangle = \sum_b \int_{-\infty}^{t} \mathrm{d}t' \int \mathrm{d}\boldsymbol{r}'\, \chi_{ab}(\boldsymbol{r}-\boldsymbol{r}', t-t')\, S_b^{ss'}(\boldsymbol{r}',t')\,, \tag{3.10}$$

where

$$\chi_{ab}(\boldsymbol{r}-\boldsymbol{r}', t-t') \equiv i\theta(t-t')\Big\langle\, [a(\boldsymbol{r},t), b(\boldsymbol{r}',t')]\,\Big\rangle \tag{3.11}$$

is the generalized susceptibility associated with a and b. The double Fourier transform of χ_{ab} obeys [16]

$$\chi_{ab}(\boldsymbol{q},\omega) - \chi^*_{b^\dagger a^\dagger}(\boldsymbol{q},\omega) = iK_{ab}(\boldsymbol{q},\omega)\left(1 - e^{-\beta\omega}\right)\,. \tag{3.12}$$

In the $T \to 0$ limit (see a short discussion in appendix D.2), when $1 - e^{-\beta\omega} \to 1$, we can use eq. (3.12) to rewrite the transition rate Γ, given by eq. (3.2), as

$$\Gamma = \frac{-i}{16 m_e^2 m_\chi^2} \sum_{ab} \int \frac{\mathrm{d}\boldsymbol{q}}{(2\pi)^3} \int \mathrm{d}\boldsymbol{v}\, f(\boldsymbol{v})\, \mathcal{F}_{ab}(\boldsymbol{q},\boldsymbol{v})\, (\chi_{a^\dagger b} - \chi^*_{b^\dagger a})\, (\boldsymbol{q}, \omega_{\boldsymbol{v},\boldsymbol{q}})\,, \tag{3.13}$$

with the DM velocity distribution function f defined by eq. (2.25) and $\mathcal{F}_{ab}$ given by eq. (3.3).

3.3 Kramers-Kronig relations

In the time domain, the generalized susceptibilities $\chi_{a^\dagger b}(\boldsymbol{q}, t-t')$ are causal, as one can see from their definition, eq. (3.11). In particular, this implies $\chi_{a^\dagger b}(\boldsymbol{q}, t-t') = 0$ for $t - t' < 0$. Consequently, in the (complex) frequency domain $\chi_{a^\dagger b}(\boldsymbol{q},\omega)$ is analytic in the upper-half plane, that is, for $\mathrm{Im}\,\omega \geq 0$. Apart of that, $\chi_{a^\dagger b}(\boldsymbol{q},\omega) \to 0$ for $|\omega| \to \infty$. Moreover, $\chi_{a^\dagger b}(\boldsymbol{q}, t-t')$ is real in the time domain, which implies that, as a function of $\omega \in \mathbb{R}$, $\mathrm{Re}\,\chi_{a^\dagger b}(\boldsymbol{q},\omega)$ is even while $\mathrm{Im}\,\chi_{a^\dagger b}(\boldsymbol{q},\omega)$ is odd.

Since $\chi_{a^\dagger b}(\boldsymbol{q},\omega)$ meets the above three conditions for every $\boldsymbol{q}$, it also obeys [23]

$$\mathrm{Re}\,\chi_{a^\dagger b}(\boldsymbol{q},\omega) = \frac{1}{\pi}\mathcal{P}\int_{-\infty}^{+\infty} \frac{\mathrm{d}\omega'}{\omega'-\omega}\, \mathrm{Im}\,\chi_{a^\dagger b}(\boldsymbol{q},\omega')\,, \tag{3.14a}$$

$$\mathrm{Im}\,\chi_{a^\dagger b}(\boldsymbol{q},\omega) = -\frac{1}{\pi}\mathcal{P}\int_{-\infty}^{+\infty} \frac{\mathrm{d}\omega'}{\omega'-\omega}\, \mathrm{Re}\,\chi_{a^\dagger b}(\boldsymbol{q},\omega')\,, \tag{3.14b}$$

JCAP08(2025)088

as well as

$$\int_0^{+\infty} \frac{\mathrm{d}\omega}{\omega} \,\mathrm{Im}\,\chi_{a^\dagger b}(\boldsymbol{q},\omega) = \frac{\pi}{2}\chi_{a^\dagger b}(\boldsymbol{q},0)\,. \tag{3.15}$$

The identities in eq. (3.14) are the Kramers-Kronig relations for the generalized susceptibilities $\chi_{a^\dagger b}(\boldsymbol{q},\omega)$, while eq. (3.15) extends the relation in eq. (2.22) to the case of general DM couplings.

4 Upper bound on the transition rate for general DM-electron couplings

In this section, we first analytically derive a general upper bound on the DM-induced electronic transition rate (section 4.1) and provide expressions for the interaction rate in specific effective models of DM (section 4.2). We then numerically evaluate the transition rate to associated upper bound ratio focusing on germanium, silicon, argon and xenon detectors, and on models where DM exhibits an anapole, magnetic dipole or electric dipole moment (section 4.3). This numerical analysis will allow us to assess which material is closest to saturate our general upper bound on Γ.

4.1 Derivation from the Kramers-Kronig relations

We start from an analytic derivation of a general upper bound on Γ based on the generalized Kramers-Kronig relations that apply to material responses beyond the familiar dielectric function.

Using eq. (3.15), we now show that the sum of eq. (3.13) is bounded from above. Let us recall eq. (3.13):

$$\Gamma = \frac{-i}{16 m_e^2 m_\chi^2} \sum_{ab} \int \frac{\mathrm{d}\boldsymbol{q}}{(2\pi)^3} \int \mathrm{d}\boldsymbol{v}\, f(\boldsymbol{v})\, \mathcal{F}_{ab}(\boldsymbol{q},\boldsymbol{v})\, (\chi_{a^\dagger b} - \chi^*_{b^\dagger a})\,(\boldsymbol{q},\omega_{\boldsymbol{v},\boldsymbol{q}})\,. \tag{4.1}$$

First, let us notice that the sum $\sum_{ab} \mathcal{F}_{ab}(\chi_{a^\dagger b} - \chi^*_{b^\dagger a})$ consists of contributions of the following types:

$$\mathcal{F}_{nn'}\,(\chi_{n^\dagger n'} - \chi^*_{n'^\dagger n})\,, \qquad \text{where} \quad n, n' = n_0, n_A\,, \tag{4.2a}$$

$$\sum_k \left[\mathcal{F}_{j_k n}\,(\chi_{j_k^\dagger n} - \chi^*_{n^\dagger j_k}) + \mathcal{F}_{n j_k}\,(\chi_{n^\dagger j_k} - \chi^*_{j_k^\dagger n})\right], \qquad \text{where} \quad \begin{cases} n = n_0, n_A \\ \boldsymbol{j} = \boldsymbol{j}_5, \boldsymbol{j}_M, \boldsymbol{j}_E\,, \end{cases} \tag{4.2b}$$

$$\sum_{k\ell} \mathcal{F}_{j_k j'_\ell}\,(\chi_{j_k^\dagger j'_\ell} - \chi^*_{j'^\dagger_\ell j_k})\,, \qquad \text{where} \quad \boldsymbol{j}, \boldsymbol{j}' = \boldsymbol{j}_5, \boldsymbol{j}_M, \boldsymbol{j}_E\,. \tag{4.2c}$$

Investigating the explicit forms of $\mathcal{F}_{ab}$ coefficients provided in appendix C, one can realize that $\mathcal{F}_{n_0 n_0}$, the only non-vanishing coefficient of the type $\mathcal{F}_{nn'}$ appearing in eq. (4.2a), is a scalar quantity depending on $q \equiv |\boldsymbol{q}|$, $v \equiv |\boldsymbol{v}|$, and v_q defined by eq. (2.26). In the contribution of type (4.2b), the relevant[5] coefficients $\mathcal{F}_{j_k n}(\boldsymbol{q},\boldsymbol{v})$ depend on the components of $\boldsymbol{q}$ and $\boldsymbol{v}$ in the following way:

$$\mathcal{F}_{j_k n}(\boldsymbol{q},\boldsymbol{v}) \equiv A_{\boldsymbol{j} n}(q, v, v_q)\,\frac{q_k}{q} + B_{\boldsymbol{j} n}(q, v, v_q)\, v_k\,. \tag{4.3}$$

[5] In the explicit form of $\mathcal{F}_{j_{M_k} n_0}$ and $\mathcal{F}_{n_A j_{5_k}}$, there appear linear terms of the third type, namely, those proportional to $\varepsilon_{kij}\,(q_i/q)\,v_j$. However, they vanish in the models considered by us (cf. sections 4.2.1 to 4.2.3).

JCAP08(2025)088

When deriving our results, we assume that the target material is isotropic (see appendix D.1). Consequently, when contracting the $F_{j_k n}$ with the corresponding susceptibility, only the component of $\boldsymbol{v}$ parallel to $\boldsymbol{q}$ is relevant. Therefore, instead of v_k we can equivalently use $v_q\, q_k/q$ [18] and obtain

$$\mathcal{F}_{j_k n}(\boldsymbol{q},\boldsymbol{v}) = \mathcal{F}^q_{\boldsymbol{j}n}(q,v,v_q)\,\frac{q_k}{q}\,, \tag{4.4}$$

where

$$\mathcal{F}^q_{\boldsymbol{j}n}(q,v,v_q) \equiv A_{\boldsymbol{j}n}(q,v,v_q) + v_q\, B_{\boldsymbol{j}n}(q,v,v_q)\,. \tag{4.5}$$

An analogous statement holds for $\mathcal{F}_{n j_k}$ as well. Similarly, for the contributions of type (4.2c), the relevant[6] coefficients $\mathcal{F}_{j_k j'_\ell}(\boldsymbol{q},\boldsymbol{v})$ can be expressed as

$$\mathcal{F}_{j_k j'_\ell}(\boldsymbol{q},\boldsymbol{v}) \equiv \mathcal{F}^\delta_{\boldsymbol{j}\boldsymbol{j}'}(q,v,v_q)\,\delta_{k\ell} + \mathcal{F}^{qq}_{\boldsymbol{j}\boldsymbol{j}'}(q,v,v_q)\,\frac{q_k q_\ell}{q^2}\,. \tag{4.6}$$

Consequently, the contributions given by eq. (4.2), which always are scalar functions of (q,v,v_q), can be expressed using

- the $\mathcal{F}_{n_0 n_0}$ coefficient and the new scalar coefficients $\mathcal{F}^q_{\boldsymbol{j}n}$, $\mathcal{F}^q_{n\boldsymbol{j}}$, $\mathcal{F}^\delta_{\boldsymbol{j}\boldsymbol{j}'}$, $\mathcal{F}^{qq}_{\boldsymbol{j}\boldsymbol{j}'}$,
- the $\chi_{n_0 n_0}$ susceptibility and the contracted susceptibilities $\chi^q_{\boldsymbol{j}^\dagger n}$, $\chi^q_{n^\dagger \boldsymbol{j}}$, $\chi^\delta_{\boldsymbol{j}^\dagger \boldsymbol{j}'}$, $\chi^{qq}_{\boldsymbol{j}^\dagger \boldsymbol{j}'}$ given by

$$\chi^q_{\boldsymbol{j}^\dagger n}(q,v_q) \equiv \sum_k \frac{q_k}{q}\,\chi_{j_k^\dagger n}(\boldsymbol{q},\boldsymbol{v})\,, \qquad \chi^q_{n^\dagger \boldsymbol{j}}(q,v_q) \equiv \sum_k \frac{q_k}{q}\,\chi_{n^\dagger j_k}(\boldsymbol{q},\boldsymbol{v})\,, \tag{4.7a}$$

$$\chi^\delta_{\boldsymbol{j}^\dagger \boldsymbol{j}'}(q,v_q) \equiv \sum_{k\ell} \delta_{k\ell}\,\chi_{j_k^\dagger j'_\ell}(\boldsymbol{q},\boldsymbol{v})\,, \qquad \chi^{qq}_{\boldsymbol{j}^\dagger \boldsymbol{j}'}(q,v_q) \equiv \sum_{k\ell} \frac{q_k q_\ell}{q^2}\,\chi_{j_k^\dagger j'_\ell}(\boldsymbol{q},\boldsymbol{v})\,. \tag{4.7b}$$

Since the above contracted susceptibilities are just linear combinations of the susceptibilities $\chi_{a^\dagger b}$, they also possess the analytic properties required to satisfy the Kramers-Kronig relations (3.14) and (3.15). For convenience, we also introduce the primed contracted susceptibilities, defined with the indices reversed:

$$\chi'_{n_0 n_0} \equiv \chi_{n_0 n_0}\,, \qquad \chi^{q\prime}_{\boldsymbol{j}^\dagger n} \equiv \chi^q_{n^\dagger \boldsymbol{j}}\,, \qquad \chi^{q\prime}_{n^\dagger \boldsymbol{j}} \equiv \chi^q_{\boldsymbol{j}^\dagger n}\,, \qquad \chi^{x\prime}_{\boldsymbol{j}^\dagger \boldsymbol{j}'} \equiv \chi^x_{\boldsymbol{j}'^\dagger \boldsymbol{j}}\,, \tag{4.8a}$$

where $x = \delta, qq$.

In the following derivation of the theoretical upper bound, each $\mathcal{F}_i$ denotes either the $\mathcal{F}_{n_0 n_0}$ coefficient or one[7] of the scalar coefficients $\mathcal{F}(q,v,v_q)$ introduced on the right-hand sides of eqs. (4.4) and (4.6). Then, χ_i denotes, respectively, either $\chi_{n_0 n_0}$ or the contracted

[6] Again, the term proportional to $\varepsilon_{k\ell m}\, q_m/m_e$ present in the explicit form of $\mathcal{F}_{j_{M_k} j_{M_\ell}}$ vanishes in the considered models. Moreover, the antisymmetric part of $\mathcal{F}_{j_{5_\ell} j_{5_m}}$, which is in principle non-zero, is irrelevant since it vanishes when contracted with $\operatorname{Im}\Delta\chi_{j^\dagger_{5_k} j_{5_\ell}}$ which is proportional to $\delta_{k\ell}$, cf. eq. (4.42).

[7] Strictly speaking, for the $\boldsymbol{j}_5\boldsymbol{j}_5$ contribution we consider a combination $\sum_{k\ell}\delta_{k\ell}\mathcal{F}_{j_{5_k} j_{5_\ell}} = 3\mathcal{F}^\delta_{\boldsymbol{j}_5\boldsymbol{j}_5} + \mathcal{F}^{qq}_{\boldsymbol{j}_5\boldsymbol{j}_5}$. This is because $\chi_{j^\dagger_{5_k} j_{5_\ell}}$ is proportional to $\delta_{k\ell}$, as can bee observed from eq. (4.42).

JCAP08(2025)088

susceptibility given by eq. (4.7) corresponding to $\mathcal{F}_i$. Using this notation, eq. (4.1) can be rewritten as

$$\Gamma = \frac{-i}{16 m_e^2 m_\chi^2} \sum_i \int \frac{\mathrm{d}\boldsymbol{q}}{(2\pi)^3} \int \mathrm{d}\boldsymbol{v}\, f(\boldsymbol{v})\, \mathcal{F}_i(q, v, v_q)\, (\chi_i - \chi_i'^*)\, (q, v_q)\,. \tag{4.9}$$

We begin by performing the change of integration variables introduced in appendix B to obtain

$$\begin{aligned}\Gamma = \frac{-i}{32\,\pi^2 m_e^2 m_\chi^2} \sum_i \int_0^\infty \mathrm{d}q\, q^2 \int_0^\infty \mathrm{d}\omega\, \Big[&\rho^{(0)}(\omega, q)\, \mathcal{F}_i^{(0)}(q, \omega, v) \\ &+ \rho^{(2)}(\omega, q)\, \mathcal{F}_i^{(2)}(q, \omega, v)\Big]\, (\chi_i - \chi_i'^*)\, (q, \omega)\,,\end{aligned} \tag{4.10}$$

where

$$\rho^{(0)}(\omega, q) = \frac{\pi}{q} \int_{v_q}^\infty \mathrm{d}v\, v \int_{-1}^1 \mathrm{d}\cos\alpha\, f(v, \cos\alpha)\,, \tag{4.11a}$$

$$\rho^{(2)}(\omega, q) = \frac{\pi}{q} \int_{v_q}^\infty \mathrm{d}v\, v^3 \int_{-1}^1 \mathrm{d}\cos\alpha\, f(v, \cos\alpha)\,. \tag{4.11b}$$

Note that, though formally the integration in eq. (4.10) is performed over $0 < q < \infty$ and $0 < \omega < \infty$, its range is effectively limited by the DM velocity distribution f to

$$0 < q < q_{\max}\,, \qquad q_{\max} \equiv 2\, m_\chi\, (v_\oplus + v_{\mathrm{esc}})\,, \tag{4.12a}$$

$$0 < \omega < \omega_{\max}(q)\,, \qquad \omega_{\max}(q) \equiv q\, (v_\oplus + v_{\mathrm{esc}}) - \frac{q^2}{2\, m_\chi}\,, \tag{4.12b}$$

corresponding to $v_q < v < v_\oplus + v_{\mathrm{esc}}$. Moreover, the energy transfer ω is required to exceed the 1-electron ionization threshold, which subsequently imposes a threshold on the DM mass, as explained in results discussion in section 4.3.

Inspection of the explicit form of the functions $\mathcal{F}_{ab}$ given in appendix C shows that in general one has

$$\mathcal{F}_i(q, \omega, v) = \mathcal{F}_i^{(0)}(q, \omega) + v^2 \mathcal{F}_i^{(2)}(q, \omega)\,, \tag{4.13}$$

where we made explicit that $\mathcal{F}_i(q, \omega, v)$ is either independent of v, or it depends on v quadratically, cf. eq. (B.14). For readability, let us now keep only the $\mathcal{F}_i^{(0)}$ term. Calculation for the other term, which will be restored at the very end, follows analogously.

The final result for Γ must be real, and since all $\mathcal{F}_i^{(0)}$'s are real in the considered models (as can be explicitly checked basing on appendix C), the part of the integral containing the real part of $(\chi_i - \chi_i'^*)$ must vanish. We thus obtain

$$\Gamma = \frac{1}{32\pi^2 m_e^2 m_\chi^2} \sum_i \int_0^{q_{\max}} \mathrm{d}q\, q^2 \int_0^{\omega_{\max}(q)} \mathrm{d}\omega\, \rho^{(0)}(\omega, q)\, \mathcal{F}_i^{(0)}(q, \omega, v)\, \mathrm{Im}\, \Delta\chi_i(q, \omega)\,, \tag{4.14}$$

where

$$\Delta\chi_i \equiv \chi_i + \chi_i'\,, \tag{4.15}$$

JCAP08(2025)088

such that $\mathrm{Im}\,\Delta\chi_i = \mathrm{Im}(\chi_i - \chi_i'^*)$. Note that, in the definition of $\Delta\chi_i$, none of the susceptibilities is complex-conjugated, so that, similarly to each $\chi_{a^\dagger b}$, every $\Delta\chi_i(q,\omega)$ (treated as a function of ω) is analytic on the complex upper half-plane. Therefore, it also obeys the Kramers-Kronig relations.

To obtain the theoretical upper bound, we perform two consecutive estimations. Firstly, after dividing and multiply the integrand by $1 = \omega/\omega$ for further convenience, we replace the value of $\omega\,\rho^{(0)}(\omega,q)\,\mathcal{F}_i^{(0)}(q,\omega)$ by its maximum for a given q:

$$\Gamma \leq \frac{1}{32\pi^2 m_e^2 m_\chi^2} \sum_i \int_0^{q_{\max}} \mathrm{d}q\, q^2 \max_\omega \left[\omega\,\rho^{(0)}(\omega,q)\,\mathcal{F}_i^{(0)}(q,\omega)\right] \times \int_0^{\omega_{\max}(q)} \frac{\mathrm{d}\omega}{\omega}\,\mathrm{Im}\,\Delta\chi_i(q,\omega)\,. \tag{4.16}$$

If, for a given value of i, $\mathrm{Im}\,\Delta\chi_i(q,\omega)$ is non-negative for each ω, the above estimation (4.16) is (for this particular i) a trivial consequence of the fact that

$$\omega\,\rho^{(0)}(\omega,q)\,\mathcal{F}_i^{(0)}(q,\omega)\,\mathrm{Im}\,\Delta\chi_i(q,\omega) \leq \max_\omega \left[\omega\,\rho^{(0)}(\omega,q)\,\mathcal{F}_i^{(0)}(q,\omega)\right] \mathrm{Im}\,\Delta\chi_i(q,\omega)\,. \tag{4.17}$$

This is not always the case; for instance, for $q = 15\,\mathrm{keV}$ the value of the $\mathrm{Im}\,\Delta\chi^{\delta}_{\boldsymbol{j}_M^\dagger \boldsymbol{j}_M}(q,\omega)$ coupling (relevant for the anapole model) calculated for Si is negative for each ω. However, as we checked numerically, for each considered coupling and material, the integral over momenta is dominated by those values of q for which $\mathrm{Im}\,\Delta\chi_i$ is predominantly positive, so that (4.16) is satisfied.

The second step makes use of the following inequality:

$$\int_0^{\omega_{\max}(q)} \frac{\mathrm{d}\omega}{\omega}\,\mathrm{Im}\,\Delta\chi_i(q,\omega) \leq \pi\,U(q)^{-1}\,. \tag{4.18}$$

To justify the above estimation for positive $\mathrm{Im}\,\Delta\chi_i$, we first extend the integration range:

$$\int_0^{\omega_{\max}(q)} \frac{\mathrm{d}\omega}{\omega}\,\mathrm{Im}\,\Delta\chi_i(q,\omega) \leq \int_0^{\infty} \frac{\mathrm{d}\omega}{\omega}\,\mathrm{Im}\,\Delta\chi_i(q,\omega)\,, \tag{4.19}$$

and then, using the Kramers-Kronig relation (3.15), replace the integral on the right-hand side by the value at $\omega = 0$:

$$\int_0^{\omega_{\max}(q)} \frac{\mathrm{d}\omega}{\omega}\,\mathrm{Im}\,\Delta\chi_i(q,\omega) \leq \frac{\pi}{2}\,\Delta\chi_i(q,0)\,. \tag{4.20}$$

Eventually, inequality (4.18) is obtained by using the estimation

$$\Delta\chi_i(q,0) \leq 2\,U(q)^{-1}\,, \tag{4.21}$$

corresponding for $\chi_i = \chi_{n_0 n_0}$ to $\varepsilon_r^{-1} > 0$, which should be the case for most materials relevant for DM detection (see an extended discussion of this issue in [21]).

Neither condition (4.19) nor (4.21) is always satisfied; for example, (4.19) does not hold in the aforementioned case of $\mathrm{Im}\,\Delta\chi^{\delta}_{\boldsymbol{j}_M^\dagger \boldsymbol{j}_M}(q = 15\,\mathrm{keV},\omega)$ for Si, and (4.21) is broken by a factor of ca. 20 for the $\Delta\chi^{\delta}_{\boldsymbol{j}_5^\dagger \boldsymbol{j}_5}$ coupling (relevant in the anapole and the magnetic dipole

JCAP08(2025)088

model) calculated for the same material at $q = 500\,\mathrm{eV}$. However, numerical tests confirm that, for all considered materials and couplings, inequality (4.18) is always fulfilled. The reason is that, for any coupling and material, at most one of inequalities (4.19) and (4.21) is broken at a time. If the first of them is fulfilled, the estimation (4.19) is very conservative for positive $\mathrm{Im}\,\Delta\chi_i$'s, so that the final conclusion holds even though (4.21) is incorrect. Conversely, if eq. (4.19) does not hold, it means that $\mathrm{Im}\,\Delta\chi_i$ is predominantly negative, so the integral in eq. (4.18) can be limited from above by any positive value and one does not have to use (4.19) and the Kramers-Kronig relations to draw the final conclusion.

Using estimation (4.18) we obtain the following theoretical upper bound on the interaction rate:

$$\Gamma \leq \frac{1}{32\pi m_e^2 m_\chi^2} \sum_i \int_0^{q_{\max}} \mathrm{d}q\, q^2 \max_\omega \left[\omega\, \rho^{(0)}(\omega, q)\, \mathcal{F}_i^{(0)}(q, \omega)\right] U(q)^{-1}\,. \tag{4.22}$$

In the general case of $\mathcal{F}_i(q, \omega, v) = \mathcal{F}_i^{(0)}(q, \omega) + v^2 \mathcal{F}_i^{(2)}(q, \omega)$ (cf. eq. (4.13)), we apply the same procedure and find:

$$\begin{aligned}\Gamma \leq \Gamma_{\mathrm{opt}} \equiv \frac{1}{32\pi m_e^2 m_\chi^2} \sum_i \int_0^{q_{\max}} \mathrm{d}q\, q^2 \max_\omega \Big[&\omega\, \rho^{(0)}(\omega, q)\, F_i^{(0)}(q, \omega) \\ &+ \omega\, \rho^{(2)}(\omega, q)\, F_i^{(2)}(q, \omega)\Big] U^{-1}(q)\,.\end{aligned} \tag{4.23}$$

Eq. (4.23) gives the theoretical upper bound on Γ we find from the Kramers-Kronig relations. It is worth noting that due to the absence of χ in the final result, this bound is independent of the choice of the detector material. Thus, a comparison of the actual interaction rate (4.14) with the result of eq. (4.23) provides a way to evaluate the given material as a potential target in direct detection experiments. Below, we apply this general bound to the specific case of anapole, magnetic dipole, and electric dipole DM.

4.1.1 DM of spins different than 1/2

In our analysis, we assume the dark particles to have spin 1/2. Effective theory of interactions of DM of spin up to 1 with nucleons or electrons has been the topic of numerous works, including [24–26]. As can be observed from table 1 of [26], to describe interactions between spin-1 DM and electrons one must employ more types of effective operators than in the fermion DM case. This would affect our calculations in two ways:

1. coefficients F_{ab} for $a, b = n_0, n_A, \boldsymbol{j}_5, \boldsymbol{j}_M, \boldsymbol{j}_E$, given by eqs. (C.1), (C.4) and (C.6), would contain more terms coming from the new operators depending on the generalized densities and currents analysed by us;

2. some of the effective operators relevant for spin-1 DM cannot be expressed in the form of our eq. (3.1), so that including them would require indices a and b to cover a broader range of generalized densities and currents. For instance, operator $\mathcal{O}_{21}$ defined in [26] requires introducing in eq. (3.1) a term proportional to

$$\frac{i}{2m_e}\left[\overleftarrow{\nabla}_{\boldsymbol{r}_e} \cdot \boldsymbol{\mathcal{S}}_X^{\mathrm{sym}} \cdot \boldsymbol{\sigma}_e\, e^{i\boldsymbol{q}\cdot\boldsymbol{r}_e} - e^{i\boldsymbol{q}\cdot\boldsymbol{r}_e}\, \boldsymbol{\sigma}_e \cdot \boldsymbol{\mathcal{S}}_X^{\mathrm{sym}} \cdot \overrightarrow{\nabla}_{\boldsymbol{r}_e}\right], \tag{4.24}$$

JCAP08(2025)088

with $(\mathcal{S}_X^{\rm sym})^{ij} \equiv \frac{1}{2}(S_X^i S_X^j + S_X^j S_X^i)$, where $\boldsymbol{S}_X$ denotes a vector formed by the spin operators of the vector DM particle. As can be observed, such a term cannot be decomposed into a DM-related and an e^--related part in any other way than by introducing a generalized "electronic coupling tensor" $\boldsymbol{\mathcal{J}}$ given by

$$\mathcal{J}^{ij} \equiv \frac{i}{2m_e}\left[\overleftarrow{\partial}^i_{\boldsymbol{r}_e}\sigma_e^j\, e^{i\boldsymbol{q}\cdot\boldsymbol{r}_e} - e^{i\boldsymbol{q}\cdot\boldsymbol{r}_e}\,\overrightarrow{\partial}^j_{\boldsymbol{r}_e}\sigma_e^i\right] . \tag{4.25}$$

Consequently, analysis of the vector DM case requires adding new contributions to the $\mathcal{F}_i$ terms both in eq. (4.14), which expresses the actual DM-e^- interaction rate, and in eq. (4.23), which provides the theoretical upper bound. The ratio $\Gamma_{\rm opt}/\Gamma$ would depend on the new terms in a non-trivial way, so that it is difficult to predict to which extent our results would apply to the general vector DM case. Note that all the new contributions to the matrix element squared would be expressible in terms of the generalized susceptibilities employed in this work; no new generalized susceptibilities would be needed [26].

On the contrary, effective operators required to describe interactions of scalar DM with electrons form a subset of those employed in the fermion DM case. Therefore, adjusting our calculations to the spin-0 case would be straightforward, as it only requires dropping terms specific to the spin-1/2 case. However, precise values of the final ratio between the theoretical optimum and the actual interaction rate cannot be predicted prior to an actual calculation.

Regardless of the aforementioned differences in detailed forms of expressions and numerical results, the methodology we have used remains valid for any spin of DM particles, so that it can be straightforwardly extended and used to generalize our approach to the cases of DM of spins other than 1/2.

4.2 Interaction rate in specific effective models

4.2.1 Anapole

DM has an anapole moment if it couples to the photon via the higher order electromagnetic coupling,

$$\mathscr{L} = \frac{1}{2}\frac{g}{\Lambda^2}\overline{\chi}\gamma^\mu\gamma^5\chi\,\partial^\nu F_{\mu\nu}\,, \tag{4.26}$$

where $F_{\mu\nu}$ is the electromagnetic field strength tensor, χ is a Majorana four-component spinor describing the DM particle, g is a coupling constant while Λ is an energy scale. In the non-relativistic limit, eq. (4.26) implies the following amplitude for DM scattering by a free electron [17],

$$\mathscr{M} = \frac{4eg}{\Lambda^2}m_\chi m_e\left[2\left(\boldsymbol{v}_{\rm el}^\perp\cdot\xi^{\dagger s'}\boldsymbol{S}_\chi\xi^s\right)\delta^{r'r} + g_e\left(\xi^{\dagger s'}\boldsymbol{S}_\chi\xi^s\right)\cdot\left(i\frac{\boldsymbol{q}}{m_e}\times\xi^{\dagger r'}\boldsymbol{S}_e\xi^r\right)\right] , \tag{4.27}$$

where $\boldsymbol{S}_\chi \equiv \boldsymbol{\sigma}_\chi/2$ ($\boldsymbol{S}_e \equiv \boldsymbol{\sigma}_e/2$) denotes the spin matrix corresponding to the dark particle (electron), $g_e = 2$, and $\boldsymbol{v}_{\rm el}^\perp$ is the so-called transverse relative velocity, which is the component of the relative DM-e^- velocity transverse to the momentum transfer in the case of elastic scattering. The associated transition potential depends on the electron density, paramagnetic current, and spin current [16]:

$$V_{\rm eff}^{ss'} = -\frac{1}{4m_e m_\chi V}\left[F_0^{ss'}n_0(-\boldsymbol{q}) + \boldsymbol{F}_5^{ss'}\cdot\boldsymbol{j}_5(-\boldsymbol{q}) + \boldsymbol{F}_M^{ss'}\cdot\boldsymbol{j}_M(-\boldsymbol{q})\right] . \tag{4.28}$$

JCAP08(2025)088

where the functions $F_0^{ss'}$, $\boldsymbol{F}_5^{ss'}$ and $\boldsymbol{F}_M^{ss'}$ are listed in eq. (C.1) with c_8 and c_9 explicitly given by

$$c_8 = 8 e m_e m_\chi \frac{g}{\Lambda^2}\,, \tag{4.29a}$$

$$c_9 = -8 e m_e m_\chi \frac{g}{\Lambda^2}\,, \tag{4.29b}$$

and all other coupling constants set to zero. By combining eqs. (4.14), (4.29) and (C.4), we find

$$\Gamma = \frac{1}{32\pi^2 m_e^2 m_\chi^2} \sum_i \int_0^{q_{\max}} \mathrm{d}q\, q^2 \int_0^{\omega_{\max}(q)} \mathrm{d}\omega\ \mathrm{Im}\,\Delta\chi_i(q,\omega) \left[\rho^{(0)}(\omega,q)\,\mathcal{F}_i^{(0)}(q,\omega) + \rho^{(2)}(\omega,q)\,\mathcal{F}_i^{(2)}(q,\omega)\right], \tag{4.30}$$

with $\mathcal{F}_i^{(0)}$, $\mathcal{F}_i^{(2)}$ defined in eq. (4.13), and the non-zero $\mathcal{F}_i$ coefficients being

$$\mathcal{F}_{n_0 n_0}(q,\omega,v) = \frac{1}{4}\left(v^2 - \frac{\omega}{2\,m_\chi} - \frac{q^2}{4\,m_\chi^2}\right) c_8^2\,, \tag{4.31a}$$

$$3\,\mathcal{F}^{\delta}_{\boldsymbol{j}_5\boldsymbol{j}_5}(q,\omega,v) + \mathcal{F}^{qq}_{\boldsymbol{j}_5\boldsymbol{j}_5}(q,\omega,v) = \sum_k \mathcal{F}_{j_{5_k}\,j_{5_k}}(q,\omega,v) = \frac{1}{8}\frac{q^2}{m_e^2}\,c_9^2\,, \tag{4.31b}$$

$$\mathcal{F}^{\delta}_{\boldsymbol{j}_M\boldsymbol{j}_M}(q,\omega,v) = \frac{1}{4}\,c_8^2\,, \tag{4.31c}$$

$$\mathcal{F}^{q}_{\boldsymbol{j}_M n_0}(q,\omega,v) = \mathcal{F}^{q}_{n_0\boldsymbol{j}_M}(q,\omega,v) = -\frac{1}{4}\frac{\omega}{q}\,c_8^2\,. \tag{4.31d}$$

4.2.2 Magnetic dipole

The Lagrangian for the magnetic dipole coupling between a Dirac DM field ψ and the photon field A_μ is

$$\mathscr{L} = \frac{g}{\Lambda}\,\overline{\psi}\sigma^{\mu\nu}\psi\,F_{\mu\nu}\,, \tag{4.32}$$

where $F_{\mu\nu} = \partial_\mu A_\nu - \partial_\nu A_\mu$, and $\sigma^{\mu\nu} = i[\gamma^\mu,\gamma^\nu]/2$. The associated amplitude for DM-electron scattering is

$$\mathscr{M} = \frac{eg}{\Lambda}\left\{4 m_e \delta^{s's}\delta^{r'r} + \frac{16 m_\chi m_e}{q^2} i\boldsymbol{q}\cdot\left(\boldsymbol{v}_{\rm el}^{\perp}\times\xi^{\dagger s'}\boldsymbol{S}_\chi\xi^s\right)\delta^{r'r} - \frac{8 g_e m_\chi}{q^2}\left[\left(\boldsymbol{q}\cdot\xi^{\dagger s'}\boldsymbol{S}_\chi\xi^s\right)\left(\boldsymbol{q}\cdot\xi^{\dagger r'}\boldsymbol{S}_e\xi^r\right) - q^2\left(\xi^{\dagger s'}\boldsymbol{S}_\chi\xi^s\right)\cdot\left(\xi^{\dagger r'}\boldsymbol{S}_e\xi^r\right)\right]\right\}, \tag{4.33}$$

with $\boldsymbol{S}_{\chi,e}$ and $\boldsymbol{v}_{\rm el}^{\perp}$ defined as in eq. (4.27). This amplitude implies an effective transition potential of the same form as in eq. (4.28), but the only coupling constants that are now

JCAP08(2025)088

different from zero are

$$c_1 = 4em_e\frac{g}{\Lambda}\,, \tag{4.34a}$$

$$c_4 = 16em_\chi\frac{g}{\Lambda}\,, \tag{4.34b}$$

$$c_5 = \frac{16em_e^2m_\chi}{q^2}\frac{g}{\Lambda}\,, \tag{4.34c}$$

$$c_6 = -\frac{16em_e^2m_\chi}{q^2}\frac{g}{\Lambda}\,. \tag{4.34d}$$

By combining eqs. (4.14), (4.34) and (C.4), we obtain a transition rate formula with the same structure as in eq. (4.30), but the non-vanishing $\mathcal{F}_i$ coefficients are now given by

$$\mathcal{F}_{n_0n_0}(q,\omega,v) = c_1^2 + \frac{q^2\,v^2 - \left(\omega + \frac{q^2}{2\,m_\chi}\right)^2}{4\,m_e^2}\,c_5^2\,, \tag{4.35a}$$

$$\begin{aligned} 3\,\mathcal{F}^{\delta}_{\boldsymbol{j}_5\boldsymbol{j}_5}(q,\omega,v) + \mathcal{F}^{qq}_{\boldsymbol{j}_5\boldsymbol{j}_5}(q,\omega,v) &= \sum_k \mathcal{F}_{j_{5_k}\,j_{5_k}}(q,\omega,v) \\ &= \frac{3}{16}c_4^2 + \frac{q^4}{16m_e^4}c_6^2 + \frac{q^2}{8m_e^2}c_4c_6\,, \end{aligned} \tag{4.35b}$$

$$\mathcal{F}^{\delta}_{\boldsymbol{j}_M\boldsymbol{j}_M}(q,\omega,v) = \frac{q^2}{4m_e^2}\,c_5^2\,, \tag{4.35c}$$

$$\mathcal{F}^{qq}_{\boldsymbol{j}_M\boldsymbol{j}_M}(q,\omega,v) = -\frac{q^2}{4m_e^2}\,c_5^2\,. \tag{4.35d}$$

4.2.3 Electric dipole

The case of electric dipole DM is characterized by the Lagrangian

$$\mathscr{L}_{\text{electric}} = \frac{g}{\Lambda}\,i\overline{\psi}\sigma^{\mu\nu}\gamma^5\psi\,F_{\mu\nu}\,. \tag{4.36}$$

The associated amplitude for DM-electron scattering takes the form

$$\mathscr{M} = \frac{eg}{\Lambda}\frac{16m_\chi m_e}{q^2}i\boldsymbol{q}\cdot\left(\xi^{\dagger s'}\boldsymbol{S}_\chi\xi^s\right)\delta^{r'r}\,. \tag{4.37}$$

This implies that the total transition rate Γ can be written as

$$\Gamma = \frac{1}{16\pi^2m_e^2m_\chi^2}\int_0^{q_{\max}}\mathrm{d}q\,q^2\int_0^{\omega_{\max}(q)}\mathrm{d}\omega\,\rho^{(0)}(\omega,q)\,\mathcal{F}_{n_0n_0}(q,\omega)\,\mathrm{Im}\,\chi_{n_0n_0}(q,\omega)\,, \tag{4.38}$$

with

$$\mathcal{F}_{n_0n_0}(q,\omega) = \frac{q^2}{4m_e^2}c_{11}^2\,, \tag{4.39}$$

where

$$c_{11} = \frac{16em_\chi m_e^2}{q^2}\frac{g}{\Lambda}\,. \tag{4.40}$$

JCAP08(2025)088

4.3 Numerical results

In order to numerically evaluate the transition rate formulae in eqs. (4.30) and (4.38), and the associated theoretical upper bound in eq. (4.23), we use the relations between the relevant generalized susceptibilities of [16], $\chi_{a^\dagger b}$, and the atomic and crystal responses (i.e., W functions) derived in [17], to express the contracted susceptibilities defined in eq. (4.7) as

$$\operatorname{Im}\chi_{n_0n_0}(q,\omega) = \frac{\operatorname{Im}\Sigma_{n_0n_0}(q,\omega)}{|1+U(q)\,[1-G(q)]\,\Sigma_{n_0n_0}(q,\omega)|^2}\,, \tag{4.41a}$$

$$\operatorname{Im}\Delta\chi^{qq}_{\boldsymbol{j}_5^\dagger\boldsymbol{j}_5}(q,\omega) = \frac{1}{3}\operatorname{Im}\Delta\chi^{\delta}_{\boldsymbol{j}_5^\dagger\boldsymbol{j}_5}(q,\omega) = 2\operatorname{Im}\Sigma_{n_0n_0}(q,\omega)\,, \tag{4.41b}$$

$$\begin{aligned}\operatorname{Im}\Delta\chi^{\delta}_{\boldsymbol{j}_M^\dagger\boldsymbol{j}_M}(q,\omega) &= \sum_{k\ell}\delta_{k\ell}\operatorname{Im}\Delta\chi_{j^\dagger_{M_k}j_{M_\ell}}(q,\omega)\\ &= \frac{2\pi^2\widetilde{\Omega}}{\omega}\left[\frac{q^2}{4m_e^2}W_1(q,\omega)+W_3(q,\omega)+\operatorname{Re}W_2(q,\omega)\right]\\ &\quad-2\,\frac{\omega^2}{q^2}\left[\operatorname{Im}\Sigma_{n_0n_0}(q,\omega)-\operatorname{Im}\chi_{n_0n_0}(q,\omega)\right]\,,\end{aligned} \tag{4.41c}$$

$$\begin{aligned}\operatorname{Im}\Delta\chi^{qq}_{\boldsymbol{j}_M^\dagger\boldsymbol{j}_M}(q,\omega) &= \sum_{k\ell}\frac{q_kq_\ell}{q^2}\operatorname{Im}\Delta\chi_{j^\dagger_{M_k}j_{M_\ell}}(q,\omega)\\ &= \frac{2\pi^2\widetilde{\Omega}}{\omega}\left[\frac{q^2}{4\,m_e^2}W_1(q,\omega)+\frac{m_e^2}{q^2}\,W_4(q,\omega)+\operatorname{Re}W_2(q,\omega)\right]\\ &\quad-2\,\frac{\omega^2}{q^2}\left[\operatorname{Im}\Sigma_{n_0n_0}(q,\omega)-\operatorname{Im}\chi_{n_0n_0}(q,\omega)\right]\,,\end{aligned} \tag{4.41d}$$

$$\begin{aligned}\operatorname{Im}\Delta\chi^{q}_{\boldsymbol{j}_M^\dagger n_0}(q,\omega) &= \sum_{k}\frac{q_k}{q}\operatorname{Im}\Delta\chi_{j^\dagger_{M_k}n_0}(q,\omega)\\ &= \frac{m_e}{q}\,\frac{\pi^2\widetilde{\Omega}}{\omega}\left[\frac{q^2}{m_e^2}W_1(q,\omega)+2\operatorname{Re}W_2(q,\omega)\right]\\ &\quad-2\,\frac{\omega}{q}\left[\operatorname{Im}\Sigma_{n_0n_0}(q,\omega)-\operatorname{Im}\chi_{n_0n_0}(q,\omega)\right]\,.\end{aligned} \tag{4.41e}$$

The result for $\operatorname{Im}\Delta\chi^{q}_{n_0\boldsymbol{j}_M}$ is the same as the one obtained for $\operatorname{Im}\Delta\chi^{q}_{\boldsymbol{j}_M^\dagger n_0}$, given by eq. (4.41e). Let us also notice that before contraction, the $\operatorname{Im}\Delta\chi_{j^\dagger_{5_k}j_{5_l}}$ susceptibility is proportional to the delta function [16]:

$$\operatorname{Im}\Delta\chi_{j^\dagger_{5_k}j_{5_\ell}}(q,\omega) = 2\,\delta_{k\ell}\operatorname{Im}\Sigma_{n_0n_0}(q,\omega)\,, \tag{4.42}$$

which was important for the reasoning of footnotes 6 and 7. In eqs. (4.41) and (4.42), we express the in-medium corrections via the density-density response function $\Sigma_{n_0n_0}$ and the local-field factor G [16]. Our derivation assumes that the material is non-spin-polarized, which allows for simplifications in the electron spin sums, resulting in the presented relation between the susceptibilities and the electron number density. For non-spin-polarized materials, $\Sigma_{j_\alpha n_0}$ and $\Sigma_{n_0 j_\beta}$ are different from zero only for $j_\alpha, j_\beta \in \{j_M, n_0\}$ [16]. The relation between $\Sigma_{n_0n_0}$ and the numerical data is explained below. $\widetilde{\Omega}$ is defined so that $\widetilde{\Omega}V/M = 1/\widetilde{m}$, where M is

JCAP08(2025)088

the detector mass and $\widetilde{m}$ is the unit cell mass in the case of crystals, and the argon or xenon atom mass in the case of noble liquids [16].[8] This implies that the total electronic transition rate per unit detector mass induced by $n_\chi V$ DM particles, i.e., $n_\chi V\Gamma/M$, is independent of V. Here, n_χ is the local DM number density.

For the functions $\mathrm{Re}\, W_2$, W_3, and W_4, we use values that were tabulated in [17] with DarkART [27][9] for argon and xenon detectors, and in [18] with QEdark-EFT [29] for germanium and silicon targets. The W_1 function is related to the imaginary part of the density-density response function, $\Sigma_{n_0 n_0}$, in the following way:

$$\mathrm{Im}\,\Sigma_{n_0 n_0}(q,\omega) = \frac{\pi^2\,\widetilde{\Omega}}{\omega}\, W_1(q,\omega)\,. \tag{4.43}$$

For crystal detectors, we extract the density-density response function $\Sigma_{n_0 n_0}$ from the equation

$$\Sigma_{n_0 n_0}(q,\omega) = U(q)^{-1}\left[\varepsilon_r^{\mathrm{GPAW}}(q,\omega) - 1\right]\,, \tag{4.44}$$

where the dielectric function $\varepsilon_r^{\mathrm{GPAW}}$ was calculated in [15] using GPAW [30], and implemented in DarkELF [31]. The W_1 function is then obtained from eq. (4.43). Conversely, in the case of argon and xenon, we use the values of W_1 tabulated in [18] to calculate the imaginary part of $\Sigma_{n_0 n_0}$. The real part of $\Sigma_{n_0 n_0}$ can be obtained from the imaginary one by applying the general Kramers-Kronig relation given by eq. (3.14).[10] For G we use the expressions in eq. (94) of [16] for germanium and silicon, while we set $G = 0$ for argon and xenon.

Figures 1 to 3 show the ratio between the optimal total interaction rate Γ_{opt}, given by eq. (4.23), and the actual total interaction rate Γ, obtained for a given material from eq. (4.14). The results presented in figure 1 have been obtained in the electric dipole model, described briefly in section 4.2.3, while figures 2 and 3 correspond to the magnetic dipole (section 4.2.2) and anapole (section 4.2.1) models, respectively. In each plot, the thick green line represents the values obtained for silicon, the thin black line corresponds to germanium, the dotted blue line denotes the results for xenon and the dashed orange line has been obtained for argon. The horizontal red line marks the reference value of 1, for which the actual interaction rate Γ would saturate the theoretical upper bound Γ_{opt}. Note that Γ_{opt} does not depend on the chosen material, so the plotted ratio can serve as an evaluation of a given material's quality with respect to its usefulness in direct searches for DM.

[8] In the case of crystals, $\widetilde{\Omega} = V_{\mathrm{cell}}^{-1}$.

[9] The $\mathrm{Re}\, W_2$ function computed by DarkART has to be multiplied by a factor of minus 1 to account for a missing minus sign in the definition of the vectorial form factor $\boldsymbol{f}_{i\to f}$ in [17]. The correct definition for $\boldsymbol{f}_{i\to f}$ is

$$\boldsymbol{f}_{i\to f}(\boldsymbol{q}) = -\frac{i}{m_e}\int \mathrm{d}\boldsymbol{r}\,\psi_f^*(\boldsymbol{r}) e^{i\boldsymbol{q}\cdot\boldsymbol{r}}\nabla_{\boldsymbol{r}}\psi_i(\boldsymbol{r})\,,$$

where ψ_i and ψ_f are the initial and final electronic wave functions. Notice also that DarkART computes all W's as a function of q and k', where k' is the asymptotic momentum of the final state electron. Following [28], we use

$$W_j(q,\omega) \equiv \frac{\omega}{2\pi}\sum_{n\ell}\int\frac{\mathrm{d}k'}{k'}\, W_j^{n\ell}(k',q)\,\delta(\omega - E_{k'\ell'm'} + E_{n\ell m})\,, \qquad j = 1,2,3,4\,,$$

to convert the $W_j^{n\ell}(q,k')_i$ functions of [17] to functions of q and ω, i.e., $W_j(q,\omega)$. Here, $E_f = E_{k'\ell'm'}$ and $E_i = E_{n\ell m}$.

[10] $\Sigma_{n_0 n_0}$ satisfies all assumptions of eq. (3.14) as well as $\chi_{n_0 n_0}$.

JCAP08(2025)088

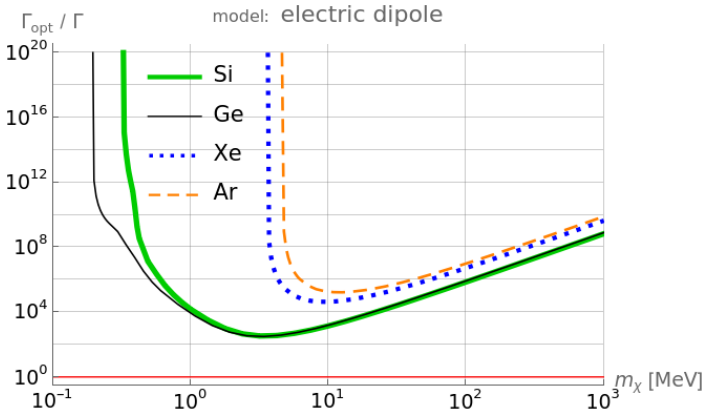

Figure 1. Ratio between the theoretical upper bound Γ_{opt} and the actual value of the interaction rate Γ, obtained within the electric dipole model, as a function of DM mass. The lines correspond to different materials: silicon (thick green), germanium (thin black), xenon (dotted blue), and argon (dashed orange). The horizontal red line marks the value of 1, for which the actual interaction rate would saturate the bound.

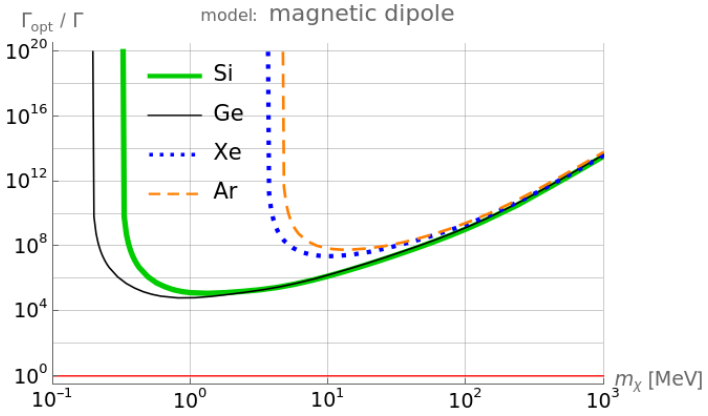

Figure 2. As in figure 1, but for the magnetic dipole model.

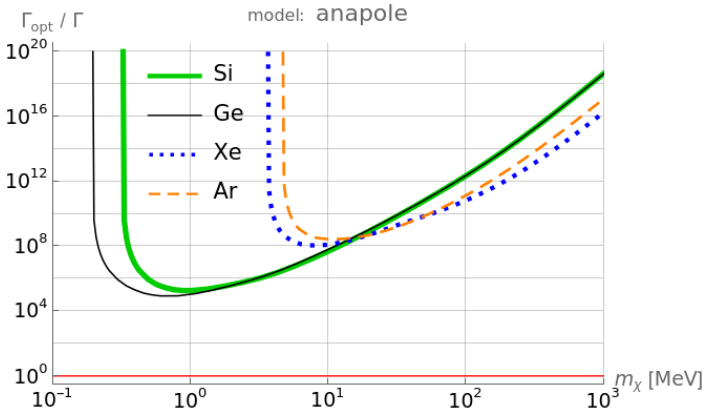

Figure 3. As in figures 1 and 2, but for the anapole model.

JCAP08(2025)088

The maximal energy transfer from a dark particle of mass m_χ, which corresponds to a total absorption of its energy, is $m_\chi \left(v_\oplus + v_{\rm esc}\right)^2 / 2$, where $v_\oplus + v_{\rm esc} \approx 800\,{\rm m/s}$ is the maximal velocity of the dark particle according to the standard halo model (see appendix A). For the materials considered in our manuscript, excitations caused by DM particles of masses lower than 0.1 MeV would fail to exceed the 1-electron ionization threshold. In such a case, the detection method should be focused on different channels, such as phononic excitations. This can clearly be observed in our plots, where the ratio between the optimum and the actual rate tends to infinity as DM mass approaches the value corresponding to the 1-electron ionization threshold: $m_\chi = 0.19\,{\rm MeV}$ for Ge, $m_\chi = 0.32\,{\rm MeV}$ for Si, $m_\chi = 4.6\,{\rm MeV}$ for Ar, $m_\chi = 3.6\,{\rm MeV}$ for Xe.

It can be observed that, for Si and Ge detectors, the ratio approaches values around 10^2 in the electric dipole model, while in the anapole and the magnetic dipole model, the ratio is always very large, i.e., above 10^4. This is correlated with the fact that the response to the density-density coupling (the only one relevant for the electric dipole) is close to the maximal possible, while the response to the $\Delta\chi^{\delta}_{\boldsymbol{j}^\dagger_M \boldsymbol{j}_M}$, $\Delta\chi^{qq}_{\boldsymbol{j}^\dagger_M \boldsymbol{j}_M}$ couplings which dominate for the anapole and the magnetic dipole, is far from optimal. In contrast, for Ar and Xe detectors, our theoretical upper bound is at least four orders of magnitude larger than the actual rate, regardless of the model. For all materials and models considered in this work, the ratio reported in figures 1 to 3 is minimal for a value of the DM particle mass in the range between 0.5 and 15 MeV.

5 Summary and conclusions

We investigated the analytic properties of the rate of DM-induced electronic transitions in materials within a framework that combines an effective theory description of DM-electron interactions with linear response theory. Within this framework, the rate of DM scattering events in materials can be expressed in terms of generalized susceptibilities describing the response of detectors to an external DM perturbation. We found that the rate of DM-induced electronic transitions in materials admits a theoretical upper bound under general assumptions on the underlying DM-electron coupling. This bound applies to models where DM couples to the electron density as well as the electron spin, paramagnetic and Rashba currents. We obtained this result by applying a set of the Kramers-Kronig relations to the generalized susceptibilities used in [16] to express the rate of DM-induced electronic transitions in materials.

We evaluated our theoretical upper bound numerically for Ar, Xe, Ge and Si targets and found that, while Ge and Si detectors are generically closer to saturate this theoretical upper bound, they are still far from saturation, unless DM couples to the electron density. This motivates the exploration of different classes of materials to effectively probe such coupling forms.

Acknowledgments

RC and MI acknowledge support from an individual research grant from the Swedish Research Council (Dnr. 2022-04299). RC has also been funded by the Knut and Alice Wallenberg

JCAP08(2025)088

Foundation, and performed this research within the "Light Dark Matter" project (Dnr. KAW 2019.0080). MI has also been supported by the Royal Society of Arts and Sciences in Gothenburg travel grant (Dnr. 2025-963).

A DM velocity distribution

We assume that the distribution of DM velocities in the laboratory frame, $f(\boldsymbol{v})$, has the form of truncated Maxwell-Boltzmann distribution,

$$f(\boldsymbol{v}) = \mathcal{N} \exp\left[-\frac{(\boldsymbol{v}+\boldsymbol{v}_\oplus)^2}{v_0^2}\right] \theta(v_{\rm esc} - |\boldsymbol{v}+\boldsymbol{v}_\oplus|)\,, \tag{A.1}$$

where $\boldsymbol{v}_\oplus$ is Earth's velocity relative to the galactic centre, $v_{\rm esc}$ is the galactic escape velocity, and v_0 is the most probable DM speed (in the galactic reference frame, in which the mean DM velocity is zero). The normalization constant $\mathcal{N}$ is given by

$$\mathcal{N} = \frac{1}{2\pi\, v_0^3}\left(\frac{\sqrt{\pi}}{2}\,\mathrm{erf}\left[\frac{v_{\rm esc}}{v_0}\right] - \frac{v_{\rm esc}}{v_0}\,\exp\left[-\frac{v_{\rm esc}^2}{v_0^2}\right]\right)^{-1}. \tag{A.2}$$

The values of $v_\oplus \equiv \boldsymbol{v}_\oplus$, $v_{\rm esc}$ and v_0 adopted in this work after [32] are

$$v_\oplus = 250.5\,\frac{\rm km}{\rm s}\,, \quad v_{\rm esc} = 544\,\frac{\rm km}{\rm s}\,, \quad v_0 = 238\,\frac{\rm km}{\rm s}\,. \tag{A.3}$$

B Integration over velocities: from d$\boldsymbol{v}$ to d$\boldsymbol{\omega}$

In general, the electronic transition rate in eq. (3.13) can be written as

$$\Gamma = \int \mathrm{d}\boldsymbol{q}\,\mathrm{d}\boldsymbol{v}\, f(\boldsymbol{v})\, B(\boldsymbol{v},\boldsymbol{q})\,, \tag{B.1}$$

where $f(\boldsymbol{v})$ describes the distribution of DM velocities in the laboratory frame (see appendix A), and $B(\boldsymbol{v},\boldsymbol{q})$ is a model dependent function we do not need to specify here. If we assume that the target material is isotropic (see appendix D.1), then

$$\Gamma = \int \mathrm{d}\boldsymbol{q}\,\mathrm{d}\boldsymbol{v}\, f(\boldsymbol{v})\, B(\omega,q,v)\,, \tag{B.2}$$

where[11]

$$\omega \equiv \boldsymbol{q}\cdot\boldsymbol{v} - \frac{q^2}{2\,m_\chi}\,. \tag{B.3}$$

Let us work in a coordinate system where Earth's velocity with respect to the galactic centre (denoted by $\boldsymbol{v}_\oplus$), DM velocity in the laboratory frame ($\boldsymbol{v}$), and momentum transfer ($\boldsymbol{q}$) are related by the following relations:

$$\boldsymbol{v}_\oplus = v_\oplus\,\boldsymbol{e}_z\,, \tag{B.4a}$$

$$\boldsymbol{v} = v\,R(\alpha,\beta)\,\boldsymbol{e}_z\,, \tag{B.4b}$$

$$\boldsymbol{q} = q\,R(\alpha,\beta)\,R(\theta,\phi)\,\boldsymbol{e}_z\,, \tag{B.4c}$$

[11] To simplify the notation, we write ω instead of $\omega_{\boldsymbol{v},\boldsymbol{q}}$, cf. eq. (2.16).

JCAP08(2025)088

where

$$R(\theta,\phi) \equiv \begin{bmatrix} \cos\phi & -\sin\phi & 0 \\ \sin\phi & \cos\phi & 0 \\ 0 & 0 & 1 \end{bmatrix} \begin{bmatrix} \cos\theta & 0 & \sin\theta \\ 0 & 1 & 0 \\ -\sin\theta & 0 & \cos\theta \end{bmatrix} \tag{B.5}$$

is a rotation matrix, so that

$$\boldsymbol{v}\cdot\boldsymbol{v}_\oplus = v v_\oplus \cos\alpha\,, \qquad\qquad \boldsymbol{v}\cdot\boldsymbol{q} = vq\cos\theta\,. \tag{B.6}$$

Next, we perform the change of integration variables $(\boldsymbol{q},\boldsymbol{v}) \to (q,\omega,v,\alpha,\beta,\phi)$, such that

$$\mathrm{d}\boldsymbol{q}\,\mathrm{d}\boldsymbol{v} = q\,\mathrm{d}q\,\mathrm{d}\omega\,v\,\mathrm{d}v\,\mathrm{d}\cos\alpha\,\mathrm{d}\beta\,\mathrm{d}\phi\,, \tag{B.7}$$

which, after integrating over the irrelevant angles β and ϕ (Γ does not depend on them), turns to

$$\mathrm{d}\boldsymbol{q}\,\mathrm{d}\boldsymbol{v} = 4\pi^2\,q\,\mathrm{d}q\,\mathrm{d}\omega\,v\,\mathrm{d}v\,\mathrm{d}\cos\alpha. \tag{B.8}$$

The integration range is

$$0<q<\infty\,, \qquad 0<\omega<\infty\,, \qquad v_q<v<\infty\,, \qquad -1<\cos\alpha<1\,, \tag{B.9}$$

where

$$v_q \equiv \frac{\omega}{q} + \frac{q}{2\,m_\chi}\,, \tag{B.10}$$

and the $\omega>0$ requirement has been introduced for physical reasons. Note that the velocity v is bounded from above by the cut-off value $v_{\rm esc}+v_\oplus$, which is imposed via the step function in $f(\boldsymbol{v})$ (see appendix A) and affects the actual range of integration over dq and $d\omega$.

B.1 Velocity-independent B

When the function B introduced in eq. (B.1) is independent of v, the rate Γ can be written as follows:

$$\Gamma = 4\pi \int_0^\infty q^2\mathrm{d}q \int_0^\infty \mathrm{d}\omega\,\rho^{(0)}(\omega,q)\,B(\omega,q)\,, \tag{B.11}$$

where

$$\rho^{(0)}(\omega,q) \equiv \frac{\pi}{q}\int_{v_q}^\infty v\,\mathrm{d}v \int_{-1}^1 \mathrm{d}\cos\alpha\,f(\boldsymbol{v})\,. \tag{B.12}$$

By analytically evaluating the angular and velocity integrals in the above equation, we find

$$\rho^{(0)}(\omega,q) = \frac{\mathcal{N}\,\pi\,v_0^2}{2\,q} \times \begin{cases} \frac{\sqrt{\pi}}{2}\,\frac{v_0}{v_\oplus}\,[\mathrm{erf}\,(x_+)+\mathrm{erf}\,(x_-)] - 2\,e^{-z^2} & \text{for } v_q < v_{\rm esc}-v_\oplus \\ \frac{\sqrt{\pi}}{2}\,\frac{v_0}{v_\oplus}\,[\mathrm{erf}\,(z)+\mathrm{erf}\,(x_-)] - (1+x_-)\,e^{-z^2} & \text{for } v_{\rm esc}-v_\oplus < v_q < v_{\rm esc}+v_\oplus \\ 0 & \text{for } v_{\rm esc}+v_\oplus < v_q, \end{cases} \tag{B.13}$$

where $x_+ \equiv (v_\oplus+v_q)/v_0$, $x_- \equiv (v_\oplus-v_q)/v_0$, $z\equiv v_{\rm esc}/v_\oplus$, and the normalization constant $\mathcal{N}$ is provided in appendix A.

JCAP08(2025)088

B.2 Velocity-dependent B

For the models studied in this work, the DM-electron scattering amplitude $\mathscr{M}$ is at most linear in $\boldsymbol{v}$. Consequently, the function B can be at most quadratic in $\boldsymbol{v}$:

$$B(\omega, q, v) = B^{(0)}(\omega, q) + B^{(2)}(\omega, q)\, v^2 \,. \tag{B.14}$$

The absence of terms linear in $\boldsymbol{v}$ follows from the fact that to contribute to a scalar function B, they must be contracted with $\boldsymbol{q}$. This product can be then expressed in terms of ω and q, see eq. (B.3). The contribution to Γ from $B^{(0)}$ has been discussed in the previous subsection. In general,

$$\begin{aligned}
\Gamma &= \int \mathrm{d}\boldsymbol{q}\, \mathrm{d}\boldsymbol{v}\, f(\boldsymbol{v})\, B(\omega, q, v) \\
&= \int \mathrm{d}\boldsymbol{q}\, \mathrm{d}\boldsymbol{v}\, f(\boldsymbol{v})\, [B^{(0)}(\omega, q) + B^{(2)}(\omega, q)\, v^2] \\
&= 4\pi \int_0^\infty q^2 \mathrm{d}q \int_0^\infty \mathrm{d}\omega\, \left[\rho^{(0)}(\omega, q)\, B^{(0)}(\omega, q) + \rho^{(2)}(\omega, q)\, B^{(2)}(\omega, q)\right] ,
\end{aligned} \tag{B.15}$$

where $\rho^{(2)}$ is defined analogously to $\rho^{(0)}$, but with an additional v^2 factor:

$$\rho^{(2)}(\omega, q) = \frac{\pi}{q} \int_{v_q}^\infty v^3\, \mathrm{d}v \int_{-1}^1 \mathrm{d}\cos\alpha\, f(\boldsymbol{v}) \,. \tag{B.16}$$

By performing the above integral analytically, we obtain

$$\begin{aligned}
\rho^{(2)}(\omega, q) &= \frac{\mathcal{N}\pi}{q} \int_{v_q}^\infty v^3\, \mathrm{d}v \int_{-1}^1 \mathrm{d}\cos\alpha\, \exp\left[-\frac{(\boldsymbol{v}+\boldsymbol{v}_\oplus)^2}{v_0^2}\right] \theta(v_{\rm esc} - |\boldsymbol{v}+\boldsymbol{v}_\oplus|) \\
&= \frac{\mathcal{N}\pi v_0^4}{4q} \begin{cases}
\frac{\sqrt{\pi}}{2}\frac{v_0}{v_\oplus}\left(1 + 2\frac{v_\oplus^2}{v_0^2}\right)[\mathrm{erf}\,(x_+) + \mathrm{erf}\,(x_-)] & \\
\quad + \left(1 - \frac{v_q}{v_\oplus}\right) e^{-x_+^2} + \left(1 + \frac{v_q}{v_\oplus}\right) e^{-x_-^2} & \text{for } v_q < v_{\rm esc} - v_\oplus \\
\quad -4\left(1 + \frac{v_{\rm esc}^2}{v_0^2} + \frac{1}{3}\frac{v_\oplus^2}{v_0^2}\right) e^{-\frac{v_{\rm esc}^2}{v_0^2}} & \\
\frac{\sqrt{\pi}}{2}\frac{v_0}{v_\oplus}\left(1 + 2\frac{v_\oplus^2}{v_0^2}\right)\left[\mathrm{erf}\left(\frac{v_{\rm esc}}{v_0}\right) + \mathrm{erf}\,(x_-)\right] & \\
\quad + \left(1 + \frac{v_q}{v_\oplus}\right) e^{-x_-^2} & \text{for } v_{\rm esc} - v_\oplus < v_q < v_{\rm esc} + v_\oplus \\
\quad -2\left[1 + \frac{1}{2}\, z + \frac{1}{3}\frac{(v_{\rm esc}+v_\oplus)^3 - v_q^3}{v_0^2\, v_\oplus}\right] e^{-\frac{v_{\rm esc}^2}{v_0^2}} & \\
0 & \text{for } v_{\rm esc} + v_\oplus < v_q,
\end{cases}
\end{aligned} \tag{B.17}$$

where, again, $x_+ \equiv (v_\oplus + v_q)/v_0$, $x_- \equiv (v_\oplus - v_q)/v_0$, $z \equiv v_{\rm esc}/v_\oplus$, and $\mathcal{N}$ is defined in appendix A.

JCAP08(2025)088

C F-functions

Below, we list explicit expressions for the functions $F_{n_0}^{ss'}$, $F_{n_A}^{ss'}$, $\boldsymbol{F}_{j_5}^{ss'}$, $\boldsymbol{F}_{j_M}^{ss'}$, and $\boldsymbol{F}_{j_E}^{ss'}$. They are given by

$$F_{n_0}^{ss'} = \xi_\chi^{s'\dagger}\left[c_1 + i\left(\frac{\boldsymbol{q}}{m_e}\times\boldsymbol{v}_\chi^\perp\right)\cdot\boldsymbol{S}_\chi c_5 + \boldsymbol{v}_\chi^\perp\cdot\boldsymbol{S}_\chi c_8 + i\frac{\boldsymbol{q}}{m_e}\cdot\boldsymbol{S}_\chi c_{11}\right]\xi^s\,, \tag{C.1a}$$

$$F_{n_A}^{ss'} = -\frac{1}{2}\xi_\chi^{s'\dagger}\left[c_7 + i\frac{\boldsymbol{q}}{m_e}\cdot\boldsymbol{S}_\chi\; c_{14}\right]\xi_\chi^s\,, \tag{C.1b}$$

$$\begin{aligned}\boldsymbol{F}_{j_5}^{ss'} = \frac{1}{2}\xi_\chi^{s'\dagger}\Bigg[&i\frac{\boldsymbol{q}}{m_e}\times\boldsymbol{v}_\chi^\perp\; c_3 + \boldsymbol{S}_\chi c_4 + \frac{\boldsymbol{q}}{m_e}\;\frac{\boldsymbol{q}}{m_e}\cdot\boldsymbol{S}_\chi c_6\\ &+\boldsymbol{v}_\chi^\perp c_7 + i\frac{\boldsymbol{q}}{m_e}\times\boldsymbol{S}_\chi c_9 + i\frac{\boldsymbol{q}}{m_e}c_{10}\\ &+\boldsymbol{v}_\chi^\perp\times\boldsymbol{S}_\chi c_{12} + i\boldsymbol{v}_\chi^\perp\frac{\boldsymbol{q}}{m_e}\cdot\boldsymbol{S}_\chi\; c_{14} + \frac{\boldsymbol{q}}{m_e}\times\boldsymbol{v}_\chi^\perp\;\frac{\boldsymbol{q}}{m_e}\cdot\boldsymbol{S}_\chi\; c_{15}\Bigg]\xi_\chi^s\,,\end{aligned} \tag{C.1c}$$

$$\boldsymbol{F}_{j_M}^{ss'} = \xi_\chi^{s'\dagger}\left[i\frac{\boldsymbol{q}}{m_e}\times\boldsymbol{S}_\chi c_5 - \boldsymbol{S}_\chi c_8\right]\xi_\chi^s\,, \tag{C.1d}$$

$$\boldsymbol{F}_{j_E}^{ss'} = \frac{1}{2}\xi_\chi^{s'\dagger}\left[\frac{\boldsymbol{q}}{m_e}\; c_3 + i\boldsymbol{S}_\chi c_{12} - i\frac{\boldsymbol{q}}{m_e}\frac{\boldsymbol{q}}{m_e}\cdot\boldsymbol{S}_\chi c_{15}\right]\xi_\chi^s\,, \tag{C.1e}$$

where

$$\boldsymbol{v}_\chi^\perp = \left(\frac{\boldsymbol{p}+\boldsymbol{p}'}{2m_\chi}\right) = \boldsymbol{v} - \frac{\boldsymbol{q}}{2m_\chi}\,, \tag{C.2}$$

$\boldsymbol{v} = \boldsymbol{p}/m_\chi$, $\boldsymbol{q} = \boldsymbol{p} - \boldsymbol{p}'$ is the momentum transferred to the electron and $\boldsymbol{S}_\chi \equiv \boldsymbol{\sigma}_\chi/2$ ($\boldsymbol{S}_e \equiv \boldsymbol{\sigma}_e/2$) denotes the spin matrix corresponding to the dark particle (electron). Elements of $\mathcal{F}_{ab}$ are defined as

$$\mathcal{F}_{ab} \equiv \frac{1}{2}\sum_{ss'} F_a^{ss'*}F_b^{ss'}\,. \tag{C.3}$$

The elements relevant for the anapole, electric dipole and magnetic dipole models investigated in this work can be explicitly expressed as

$$\mathcal{F}_{n_0n_0} = c_1^2 + \frac{1}{4}\left|\frac{\boldsymbol{q}}{m_e}\times\boldsymbol{v}_\chi^\perp\right|^2 c_5^2 + \frac{1}{4}v_\chi^{\perp 2}c_8^2 + \frac{1}{4}\frac{q^2}{m_e^2}c_{11}^2\,, \tag{C.4a}$$

$$\begin{aligned}\sum_k \mathcal{F}_{j_{5_k}j_{5_k}} = \frac{1}{4}\Bigg[&\left|\frac{\boldsymbol{q}}{m_e}\times\boldsymbol{v}_\chi^\perp\right|^2 c_3^2 + \frac{3}{4}c_4^2 + \frac{q^4}{4\,m_e^4}c_6^2 + v_\chi^{\perp 2}c_7^2 + \frac{q^2}{2m_e^2}c_9^2\\ &+\frac{q^2}{m_e^2}c_{10}^2 + \frac{v_\chi^{\perp 2}}{2}c_{12}^2 + \frac{q^2}{4m_e^2}v_\chi^{\perp 2}c_{14}^2 + \left|\frac{\boldsymbol{q}}{m_e}\times\boldsymbol{v}_\chi^\perp\right|^2\frac{q^2}{4m_e^2}c_{15}^2\\ &+\frac{q^2}{2m_e^2}c_4c_6 - \frac{1}{2}\left|\frac{\boldsymbol{q}}{m_e}\times\boldsymbol{v}_\chi^\perp\right|^2 c_{12}c_{15}\Bigg]\,,\end{aligned} \tag{C.4b}$$

$$\mathcal{F}_{j_{M_k}j_{M_\ell}} = \frac{q^2\delta_{k\ell} - q_kq_\ell}{4m_e^2}c_5^2 + \frac{1}{4}c_8^2\delta_{k\ell} - \frac{i}{2}\varepsilon_{k\ell m}\frac{q_m}{m_e}c_5c_8\,, \tag{C.4c}$$

$$\mathcal{F}_{j_{M_k}n_0} = -\frac{1}{4}v_{\chi k}^\perp c_8^2 - \frac{i}{2}\left(\frac{\boldsymbol{q}}{m_e}\times\boldsymbol{v}_\chi^\perp\right)_k c_5c_8 - \frac{i}{4}\frac{q_k}{m_e}c_8c_{11}\,. \tag{C.4d}$$

JCAP08(2025)088

Note that the expressions $(\boldsymbol{v}_\chi^\perp)^2$ and $\left|\frac{\boldsymbol{q}}{m_e}\times\boldsymbol{v}_\chi^\perp\right|^2$ can be expressed in terms of $v\equiv|\boldsymbol{v}|$, $q\equiv|\boldsymbol{q}|$ and $v_q\equiv\boldsymbol{v}\cdot\frac{\boldsymbol{q}}{q}$ as

$$(\boldsymbol{v}_\chi^\perp)^2=v^2-v_q\frac{q}{m_\chi}+\frac{q^2}{4\,m_\chi^2}\,,\qquad\qquad\left|\frac{\boldsymbol{q}}{m_e}\times\boldsymbol{v}_\chi^\perp\right|^2=\frac{q^2}{m_e^2}\left(v^2-v_q^2\right). \tag{C.5}$$

For completeness, we also list the other elements:

$$\mathcal{F}_{n_An_A}=\frac{1}{4}\left(c_7^2+\frac{1}{4}\frac{q^2}{m_e^2}c_{14}^2\right), \tag{C.6a}$$

$$\mathcal{F}_{j_{E_k}j_{E_\ell}}=\frac{1}{4}\left(\frac{q_kq_\ell}{m_e^2}c_3^2+\frac{1}{4}\delta_{k\ell}c_{12}^2+\frac{q^2}{4m_e^2}\frac{q_kq_\ell}{m_e^2}c_{15}^2-\frac{q_kq_\ell}{2m_e^2}c_{12}c_{15}\right), \tag{C.6b}$$

$$\mathcal{F}_{j_{E_k}n_A}=\frac{1}{4}\left[-\frac{q_k}{m_e}c_3c_7-\frac{q_k}{4m_e}c_{12}c_{14}+\frac{q_k}{4m_e}\frac{q^2}{m_e^2}c_{14}c_{15}\right], \tag{C.6c}$$

$$\begin{aligned}\mathcal{F}_{n_Aj_{5_k}}=&-\frac{1}{4}v_{\chi k}^\perp c_7^2-\frac{q^2}{16m_e^2}v_{\chi k}^\perp c_{14}^2-\frac{i}{4}\left(\frac{\boldsymbol{q}}{m_e}\times\boldsymbol{v}_\chi^\perp\right)_k c_3c_7-\frac{i}{4}\frac{q_k}{m_e}c_7c_{10}\\&+\frac{i}{16}\frac{q_k}{m_e}c_4c_{14}+\frac{i}{16}\frac{q^2}{m_e^2}\frac{q_k}{m_e}c_6c_{14}+\frac{i}{16}\frac{q^2}{m_e^2}\left(\frac{\boldsymbol{q}}{m_e}\times\boldsymbol{v}_\chi^\perp\right)_k c_{14}c_{15}\,,\end{aligned} \tag{C.6d}$$

$$\begin{aligned}\varepsilon_{k\ell m}\mathcal{F}_{j_{5_\ell}j_{E_m}}=\frac{1}{4}\Bigg[&i\frac{q_k\boldsymbol{q}\cdot\boldsymbol{v}_\chi^\perp-q^2v_{\chi k}^\perp}{m_e^2}c_3^2-\frac{i}{2}v_{\chi k}^\perp c_{12}^2+\frac{i}{4}\frac{\boldsymbol{q}\cdot\boldsymbol{v}_\chi^\perp q_k-q^2v_{\chi k}^\perp}{m_e^2}\frac{q^2}{m_e^2}c_{15}^2\\&-\left(\frac{\boldsymbol{q}}{m_e}\times\boldsymbol{v}_\chi^\perp\right)_k c_3c_7-\frac{q_k}{2m_e}c_9c_{12}-\frac{5i}{4}\frac{\boldsymbol{q}\cdot\boldsymbol{v}_\chi^\perp q_k-q^2v_{\chi k}^\perp}{m_e^2}c_{12}c_{15}\\&-\left(\frac{\boldsymbol{q}}{m_e}\times\boldsymbol{v}_\chi^\perp\right)_k c_{12}c_{14}+\frac{q^2}{4m_e^2}\left(\frac{\boldsymbol{q}}{m_e}\times\boldsymbol{v}_\chi^\perp\right)_k c_{14}c_{15}\Bigg].\end{aligned} \tag{C.6e}$$

D On the isotropy and $T\to 0$ assumptions

D.1 Isotropy of the material

Following [16], in our derivation we assume isotropy of the detector material. This assumption allows us to:

- integrate out most of the angular variables in appendix B,
- neglect the screening corrections to the transverse responses [16].

Although the assumption of isotropy is not always strictly satisfied, it is often satisfied approximately, to the extent that allows us to neglect the local-field [15] and the screening [18] corrections.

For isotropic and non-spin-polarized materials, the results provided in this work are exact. As we point out above eq. (2.27), below eq. (4.3), and above eq. (B.2), the assumption of isotropy is mathematically equivalent to averaging over detector's orientation. Thus, for non-isotropic materials, the results correspond to an expected value given the detector's orientation is chosen randomly, or to a situation in which the orientation changes cyclically

JCAP08(2025)088

(e.g., the detector is rotating). This standard approach has been also used and extensively discussed in, e.g., [13, 18, 21].

D.2 Temperature dependence of the results

In our results, the thermal corrections are encoded in the exponential term $e^{-\beta\omega}$ in eq. (3.12). The detectors of interest are assumed to operate in temperatures not exceeding the room temperature, equivalent to ca. 0.025 eV. This value is very small in comparison to the smallest energies considered in our manuscript, e.g., the one-electron ionization threshold of germanium is 0.67 eV. Hence, the exponential term in eq. (3.12) is completely negligible in comparison with 1, which justifies using the limit $T \to 0$.

For metals, not considered in our manuscript, those effects could be of some relevance because of the absence of the band gap whose energy would have to be exceeded to induce a signal. For instance, for energy transfer equal to 1 meV, the value of the $(1 - e^{-\beta\omega})$ term in eq. (3.12) becomes $0.04 \ll 1$. Nevertheless, to obtain the total interaction rate we integrate over the whole range of allowed ω's, so that the higher values, with negligible thermal term, should dominate the result and the thermal correction should not significantly affect the ratio between the actual interaction rate and the theoretical optimum.

One should definitely take into account the thermal effects described by the $e^{-\beta\omega}$ term when considering phononic detection channel, for which even the smallest energies may be relevant and could provide a measurable signal. This case is, however, beyond the scope of this work.

References

[1] M. Battaglieri et al., *U.S. Cosmic Visions: New Ideas in Dark Matter 2017: Community Report*, in the proceedings of the *U.S. Cosmic Visions: New Ideas in Dark Matter*, College Park, U.S.A., 23–25 March 2017, FERMILAB-CONF-17-282-AE-PPD-T (2017) [arXiv:1707.04591] [INSPIRE].

[2] A. Mitridate, T. Trickle, Z. Zhang and K.M. Zurek, *Snowmass white paper: Light dark matter direct detection at the interface with condensed matter physics*, *Phys. Dark Univ.* **40** (2023) 101221 [arXiv:2203.07492] [INSPIRE].

[3] S. Balan et al., *Resonant or asymmetric: the status of sub-GeV dark matter*, *JCAP* **01** (2025) 053 [arXiv:2405.17548] [INSPIRE].

[4] B.W. Lee and S. Weinberg, *Cosmological Lower Bound on Heavy Neutrino Masses*, *Phys. Rev. Lett.* **39** (1977) 165 [INSPIRE].

[5] EDELWEISS collaboration, *First germanium-based constraints on sub-MeV Dark Matter with the EDELWEISS experiment*, *Phys. Rev. Lett.* **125** (2020) 141301 [arXiv:2003.01046] [INSPIRE].

[6] SENSEI collaboration, *First Direct-Detection Results on Sub-GeV Dark Matter Using the SENSEI Detector at SNOLAB*, *Phys. Rev. Lett.* **134** (2025) 011804 [arXiv:2312.13342] [INSPIRE].

[7] DAMIC-M collaboration, *First Constraints from DAMIC-M on Sub-GeV Dark-Matter Particles Interacting with Electrons*, *Phys. Rev. Lett.* **130** (2023) 171003 [arXiv:2302.02372] [INSPIRE].

JCAP08(2025)088

[8] SuperCDMS collaboration, *Light dark matter constraints from SuperCDMS HVeV detectors operated underground with an anticoincidence event selection*, *Phys. Rev. D* **111** (2025) 012006 [arXiv:2407.08085] [INSPIRE].

[9] DarkSide collaboration, *Search for Dark Matter Particle Interactions with Electron Final States with DarkSide-50*, *Phys. Rev. Lett.* **130** (2023) 101002 [arXiv:2207.11968] [INSPIRE].

[10] XENON collaboration, *Search for New Physics in Electronic Recoil Data from XENONnT*, *Phys. Rev. Lett.* **129** (2022) 161805 [arXiv:2207.11330] [INSPIRE].

[11] J. Kopp, V. Niro, T. Schwetz and J. Zupan, *DAMA/LIBRA and leptonically interacting Dark Matter*, *Phys. Rev. D* **80** (2009) 083502 [arXiv:0907.3159] [INSPIRE].

[12] R. Essig, J. Mardon and T. Volansky, *Direct Detection of Sub-GeV Dark Matter*, *Phys. Rev. D* **85** (2012) 076007 [arXiv:1108.5383] [INSPIRE].

[13] R. Essig, M. Fernandez-Serra, J. Mardon, A. Soto, T. Volansky and T.-T. Yu, *Direct Detection of sub-GeV Dark Matter with Semiconductor Targets*, *JHEP* **05** (2016) 046 [arXiv:1509.01598] [INSPIRE].

[14] Y. Hochberg, Y. Kahn, N. Kurinsky, B.V. Lehmann, T.C. Yu and K.K. Berggren, *Determining Dark-Matter-Electron Scattering Rates from the Dielectric Function*, *Phys. Rev. Lett.* **127** (2021) 151802 [arXiv:2101.08263] [INSPIRE].

[15] S. Knapen, J. Kozaczuk and T. Lin, *Dark matter-electron scattering in dielectrics*, *Phys. Rev. D* **104** (2021) 015031 [arXiv:2101.08275] [INSPIRE].

[16] R. Catena and N.A. Spaldin, *Linear response theory for light dark matter-electron scattering in materials*, *Phys. Rev. Res.* **6** (2024) 033230 [arXiv:2402.06817] [INSPIRE].

[17] R. Catena, T. Emken, N.A. Spaldin and W. Tarantino, *Atomic responses to general dark matter-electron interactions*, *Phys. Rev. Res.* **2** (2020) 033195 [*Erratum ibid.* **7** (2025) 019001] [arXiv:1912.08204] [INSPIRE].

[18] R. Catena, T. Emken, M. Matas, N.A. Spaldin and E. Urdshals, *Crystal responses to general dark matter-electron interactions*, *Phys. Rev. Res.* **3** (2021) 033149 [arXiv:2105.02233] [INSPIRE].

[19] T. Trickle, Z. Zhang and K.M. Zurek, *Effective field theory of dark matter direct detection with collective excitations*, *Phys. Rev. D* **105** (2022) 015001 [arXiv:2009.13534] [INSPIRE].

[20] G. Krnjaic, D. Rocha and T. Trickle, *The non-relativistic effective field theory of dark matter-electron interactions*, *JHEP* **03** (2025) 165 [arXiv:2407.14598] [INSPIRE].

[21] R. Lasenby and A. Prabhu, *Dark matter-electron scattering in materials: Sum rules and heterostructures*, *Phys. Rev. D* **105** (2022) 095009 [arXiv:2110.01587] [INSPIRE].

[22] H. Tatewaki, S. Yamamoto and Y. Hatano, *Relativistic Effects in the Electronic Structure of Atoms*, *ACS Omega* **2** (2017) 6072.

[23] J. Solyom, *Fundamentals of the physics of solids*, Springer, Berlin, Germany (2011).

[24] P. Gondolo, I. Jeong, S. Kang, S. Scopel and G. Tomar, *Phenomenology of nuclear scattering for a WIMP of arbitrary spin*, *Phys. Rev. D* **104** (2021) 063018 [arXiv:2102.09778] [INSPIRE].

[25] P. Gondolo, S. Kang, S. Scopel and G. Tomar, *Effective theory of nuclear scattering for a WIMP of arbitrary spin*, *Phys. Rev. D* **104** (2021) 063017 [arXiv:2008.05120] [INSPIRE].

[26] J.-H. Liang, Y. Liao, X.-D. Ma and H.-L. Wang, *A systematic investigation on dark matter-electron scattering in effective field theories*, *JHEP* **07** (2024) 279 [arXiv:2406.10912] [INSPIRE].

JCAP08(2025)088

[27] T. Emken, *DarkART: Version 0.1.0*, Zenodo (2021) [DOI:10.5281/zenodo.6046225].

[28] R. Catena et al., *Dark matter-electron interactions in materials beyond the dark photon model*, *JCAP* **03** (2023) 052 [arXiv:2210.07305] [INSPIRE].

[29] E. Urdshals and M. Matas, *QEdark-EFT*, Zenodo (2021) [DOI:10.5281/zenodo.4739187].

[30] J.J. Mortensen et al., *GPAW: An open Python package for electronic structure calculations*, *J. Chem. Phys.* **160** (2024) 092503.

[31] S. Knapen, J. Kozaczuk and T. Lin, *PYTHON package for dark matter scattering in dielectric targets*, *Phys. Rev. D* **105** (2022) 015014 [arXiv:2104.12786] [INSPIRE].

[32] D. Baxter et al., *Recommended conventions for reporting results from direct dark matter searches*, *Eur. Phys. J. C* **81** (2021) 907 [arXiv:2105.00599] [INSPIRE].

JCAP08(2025)088